Lead-Free Perovskites for Lighting and Lasing Applications: A Minireview

Elena V. Ushakova [1,2,*], **Sergei A. Cherevkov [1]**, **Vera A. Kuznetsova [1]** and **Alexander V. Baranov [1]**

[1]   Center of Information Optical Technologies, ITMO University, 49 Kronverksky pr., Saint Petersburg 197101, Russia; s.cherevkov@corp.ifmo.ru (S.A.C.); v.kuznetsova.a@gmail.com (V.A.K.); a_v_baranov@yahoo.com (A.V.B.)

[2]   Department of Materials Science and Engineering, and Center for Functional Photonics (CFP), City University of Hong Kong, 83 Tat Chee Avenue, Kowloon, Hong Kong, China

*   Correspondence: elena.ushakova@itmo.ru

Abstract: Research on materials with perovskite crystal symmetry for photonics applications represent a rapidly growing area of the photonics development due to their unique optical and electrical properties. Among them are high charge carrier mobility, high photoluminescence quantum yield, and high extinction coefficients, which can be tuned through all visible range by a controllable change in chemical composition. To date, most of such materials contain lead atoms, which is one of the obstacles for their large-scale implementation. This disadvantage can be overcome via the substitution of lead with less toxic chemical elements, such as Sn, Bi, Yb, etc., and their mixtures. Herein, we summarized the scientific works from 2016 related to the lead-free perovskite materials with stress on the lasing and lighting applications. The synthetic approaches, chemical composition, and morphology of materials, together with the optimal device configurations depending on the material parameters are summarized with a focus on future challenges.

Keywords: perovskite; nanocrystals; lead-free; lasing; superluminescence; LED; photonics

1. Introduction

The growing request of the market makes demands on modern photonics materials such as ability for miniaturization, higher efficiency, tunable and controllable optical and electrical properties, and stable performance. Thus, the scientific community tackles this challenge by the design and development of novel nanostructured optical materials. Among a wide variety of materials, perovskites can be highlighted thanks to their unique opto-electronic properties: High charge carrier mobility, high photoluminescence quantum yields (PLQYs), and high extinction coefficients, which can be tuned through all visible range.

Perovskite materials in common can be characterized by ABX_3 chemical formula where A is a large monovalent organic or inorganic cation, B is a divalent metal cation, X is a halide anion, or their mixture. Although this formula is relatively simple, it allows one to form materials with different composition and, hence, to achieve a wide variety of physical and chemical properties. Other modifications of the perovskite crystal structure include:

- Layered or 2D, including Ruddlesden–Popper (RP) perovskites with formula L_2BX_4 where L is organic molecule (ligand),
- Double perovskites where the 2 B is replaced by 1 atom with 1+ valence and 1 atom with 3+ valence resulting in $A_2B^+B^{3+}X_6$ structure;

- Perovskite-related crystal structures with formula A_4BX_6 or AB_2X_5.

Starting from the first reports on the perovskite materials dated back to 1839 for the discovery of $CaTiO_3$ mineral by Gustav Rose, the field was mostly devoted to the oxides with the same crystal symmetry until the investigation of cesium halides doped with Pb atoms which started in 1970s [1]. However, this topic was developed slowly and research was done only in the specific fields, since the PL quantum yield of the metal halide perovskites is quite low [2]. The first decade of XXIth century became a crucial moment of perovskite material history with observation of intense emission from the perovskite materials [3] and of extremely long lengths of charge carriers' diffusion [4].

Considering the different morphology of perovskite nanomaterials, the two main classes can be highlighted: 2D or nanoplatelets and 0D or nanocrystals. The background for 2D perovskites was established in the 1990s and was related to the layered bulk crystals which possess similar properties as free-standing nanoplatelets. In 2015 Tisdale et al. [5] showed the synthesis of stable perovskite nanoplatelets, followed by work of Sichert and co-workers [6] on $L_2[MAPbBr_3]_{n-1}PbBr_4$ nanoplatelet synthesis with controlled thickness and optical transitions. Synthetic routes for nanocrystals were developed in parallel, and in 2014, a ligand-assisted reprecipitation method to synthesize the perovskite nanocrystals was first reported [7]; a hot-injection method of lead halide perovskite nanocrystal synthesis was first introduced by the work [8] describing a synthetic route of all-inorganic perovskite nanocrystals (NCs) with high PLQY. These works burst the interest of the scientific community and entailed the increasing number of published scientific and engineering works.

Since 2009, more than 48,000 papers have been published already, and the amount of publication grows exponentially as it can be seen in Figure 1a. It is worth to mention that after 2015, a huge increase in the area devoted to perovskite nanocrystals was observed. To help a reader navigate in this ocean of information, several reviews are highlighted here to give a wide view on the perovskite-related topic.

In 2016, Q. Xiong et al. published a review [9] on synthesis and applications of metal halide perovskite nanomaterials. In this review, authors focused on precise and detailed description of the synthetic routes for nanocrystals, nanowires, and nanoplates formation, including hot-injection, ligand-assistant reprecipitation, and chemical vapor deposition methods with focus on the crystal formation mechanism. In 2018, M.V. Kovalenko, L. Manna, et al. in their review [10] highlighted the challenges and opportunities of colloidal lead-halide perovskite nanocrystals as a perspective materials to replace the conventional semiconductor quantum dots. Indeed, lead-halide perovskite NCs are believed to become as novel single-photon sources and highly efficient active down-converting media in lightning applications. The authors emphasized the existence of some ambiguities in the crystal structure, related energy structure, and contribution of different crystal phases and/or chemical composition to the NC emission. Along with the investigation of the perovskite nanocrystals, a lot of work was done in the research field devoted to 2D perovskite materials. In 2017, W. A. Tisdale et al. published a review on perovskite nanoplatelets [11], where they showed the 2D materials advantages over the bulk materials, and discussed in detail perovskite nanoplatelets synthesis, photophysics, and stability. Next, in 2018, Letian Dou et al. published a review [12] on 2D perovskite materials with extensive overview of their applications. It worth to be noted that yet another set of reviews were published in 2019 in Chemical Reviews [13–16], with the topics covered there including metal halide perovskite nanocrystals, layered halide perovskites, perovskite interfaces, and halide perovskite photovoltaics.

Although perovskite materials, in particular lead-halide perovskites, have already been implemented in different areas of photovoltaics, there are still some problems that need to be tackled. The main challenges are the increasing of the stability and mass production, and the development of the new lead-free materials. The publication analysis in Figure 1a shows that the number of papers on lead-free perovskites has also increased, especially over the last five years, and now reaches 14% from all number of papers. The solution of these problems will result in increased performance of the photovoltaic and optoelectronic devices based on the perovskite active media. In 2017, Zeijiao Shi et al. [17] reviewed the research field devoted to lead-free perovskite materials and

revealed the main trends that need to be developed: Understanding of the fundamental photophysics and finding novel synthetic routes for lead-free perovskite materials. Since then, many scientific papers were published. We want to highlight in this piece some of the recent review papers on this topic.
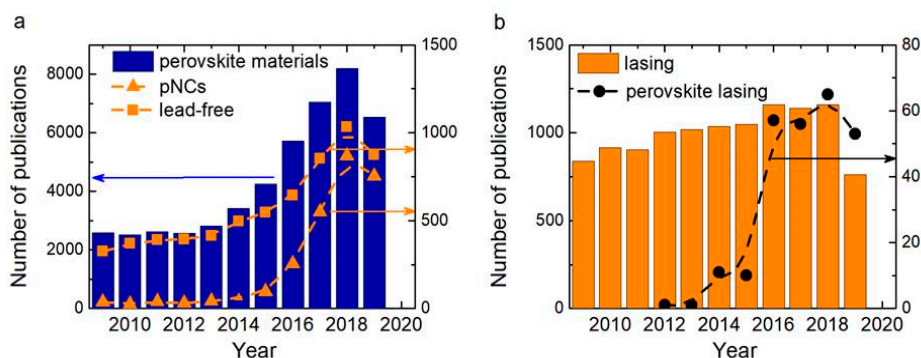

Figure 1. (**a**) Plot of publications number in the last decade: on perovskite materials (blue columns), on lead-free perovskite materials (orange squares), and on perovskite NCs (orange triangles). (**b**) Plot of publications number in the last decade: On lasing (orange columns), on lasing in perovskite materials (black circles).

In a recent review [18] by F. Sani et al., information on lead-free organic-inorganic halide perovskite solar cells was summarized. The authors inferred that the structural modification affects greatly the overall photovoltaic performance of the solar cells. Jia Sun et al. in their recent perspective [19] discussed different types of lead-free perovskite materials for future optoelectronic applications as LEDs and inferred that the working routes on the lead-based perovskites would benefit not only the developing field of light-emitting devices, but also the field of perovskite-based photovoltaics. Jiajun Luo et al. in their review [20] noted that although several types of lead-free perovskite materials were already established, there is still plenty of work to be done, including evolving the synthesis routes to achieve controllable PL peak position and PL QYs above 80%, improving the outdoor stability of operating devices, and expanding their applications towards luminescent solar concentrators and X-ray scintillators. In the lead-free perovskite family, 2D materials are highlighted by Jie Wang et al. in their recent review [21] with a focus on their perspective properties as highly luminescent phosphor for novel lightning applications.

Since the perovskite materials possess high emission quantum yields together with tunable optical transitions (properties) varying in a wide range, these materials are prospective in utilization as an amplifying media in laser systems. It is also confirmed by the increasing interest of scientific society shown by growth of publications, shown in Figure 1b. In a recent review [22] by K. Petridis et al., success in development of lasers based on organic and inorganic perovskite materials has been shown. In their review, operational principles and laser configurations were covered along with future challenges, including realization of electrically pumped perovskite lasers, stability of the optical responses during the device operating, and search for other chemical compound configurations of perovskite materials. M. L. De Giorgi and M. Anni in their review [23] focused on approaches to optimize the amplified spontaneous emission (ASE) properties in lead-halide perovskites including pumping regimes and configurations, including electrically pumped lasers.

In the present mini-review, we show recent development in the field of lead-free perovskite materials application in light-emitting devices. In the 'synthesis' section, we discuss in detail different synthetic approaches of fabrication lead-free perovskites with a focus on chemical composition and resulting morphology of materials. In the 'lasing systems' section, we discuss the morphology of perovskite materials utilized in the lasing devices with varied resonator' architecture. In the last section, we discuss recent progress in LED and lasing technologies over the last five years. Finally, we give perspectives of the development of the lead-free perovskite materials for photovoltaic applications.

2. Synthesis

2.1. Chemical Composition

Since the perovskite materials are defect-tolerant, they possess high PL quantum yields of 60% for films [24], 26% for nanoplates [25], and up to 100% for NCs [8,26,27], which inspires scientists to design new lead-free materials with the similar crystal structure.

To replace Pb (II) in halide perovskites, several low-toxic cations from the same group of periodical table and those closest to it were proposed, including Sn(II) [28–32], In (III) [33,34], Bi(III) [35–40], Sb(III) [41], and others. At the same time, the double perovskite structure gained distribution in lead-free perovskites due to the wide range of cations from III group mixed with Ag(I) [42–49]. As for the lead-based, lead-free perovskites can also be divided to organic–inorganic and all-inorganic. For organic–inorganic lead-free perovskites, standard methylammonium [39,40,50], butylamine [32], 1,3-propanediammonium [51], and phenethylammonium [52] can be used as the A cations. For all-inorganic lead-free perovskites, the most used A cation is Cs, however there are several reports on Rb and Rb/Cs mixture [29,37]. The variety of chemical composition allows tuning the optical transitions of the lead-free perovskites in a wide spectral range from 425 to 990 nm. Here, we will discuss different chemical compositions of lead-free perovskite materials and describe the synthetic methods. Detailed information on the synthesis, morphology, and optical properties of lead-free perovskites is presented in Table 1.

Table 1. Chemical formula, morphology, and optical properties of lead-free perovskite materials and their synthesis routes.

Chemical Formula	Morphology	Size *	Type of Synthesis	Abs, nm	PL, nm	PL FWHM, nm	PLQY, %	Reference
Tin-Based Perovskites								
$Cs_{1-x}Rb_xSnBr_3$	Film	N/A	Annealing	670–750	680–710	50	N/A	[29]
$Cs_2SnCl_{6-x}Br_x$	Single crystal	1–2 cm	Hydrothermal	350–750			N/A	[30]
Cs_2SnX_6 (X = Br, I)	Single crystal	3–5 μm	Hydrothermal	900	675	50	N/A	[31]
$BA_2MA_3Sn_4I_{13}$	Film	GS 9 μm	Spin-coating	850	990	75	N/A	[32]
Bismuth-Based Perovskites								
$(C_6H_5NH_3)BiI_4$	Film	area > 20 cm²	Spin-coating	525	690	30	N/A	[36]
$Rb_7Bi_3Cl_{16}$	Single crystal	18.4 × 7.2 × 6.0 mm	Hydrothermal	280	437	93	28.4	[37]
$Rb_7Bi_3Cl_{16}$	NCs	1.85 nm	LARP	280	437	93	28.4	[37]
Cs_3BiBr_6	Single crystal	30 μm	Annealing	485	475	52	19.4	[38]
$(CH_3NH_3)_3Bi_2I_9$	Film	GS 7.57 μm	Spin-coating	650			N/A	[39]
$(CH_3NH_3)_3Bi_2I_9$	Film	GS 200 nm	Spin-coating	600	575 and 605		N/A	[40]
$(PrAm)_2Bi_2I_{10}\cdot2H_2O$	Single crystal	1–10 mm	Antisolvent diffusion	600	530 and 690		N/A	[51]
$Cs_3Bi_2Br_9$	NCs	3.3 nm	Hot injection	390	600 and 620		42.4	[53]
Other Elements (In, Au, Cu, Yb)								
$Cs_2InBr_5\cdot H_2O$	Single crystal	2 mm	Hydrothermal	450	695	200	33	[34]
$(CH_3NH_3)AuX_4\cdot H_2O$, X = Cl, Br	Single crystal	5 mm	Slow evaporation	650	425	75	N/A	[50]
$Cs_3Cu_2I_5$	Film	GS 40 μm	Vapor-assisted	400	442	100	N/A	[54]
$CsYbI_3$	NCs	9.5 nm	Hot injection	660	671	50	58	[55]

Table 1. *Cont.*

Chemical Formula	Morphology	Size *	Type of Synthesis	Abs, nm	PL, nm	PL FWHM, nm	PLQY, %	Reference
			Double Perovskites					
$Cs_2AgInCl_6$	NCs	10 nm	Hot injection	300	550	250	N/A	[43]
$Cs_2AgSbCl_6$	NCs	10 nm	Hot injection	360	550	250	N/A	[43]
$Cs_2AgBiBr_6$	Film	T 200 nm	Spin-coating	440	620	50	N/A	[44]
$Cs_2AgInCl_6$	NCs	10 nm	Hot injection	390	580	125	11.4	[45]
$Cs_2AgSbBr_6$	Single crystal	1 mm	Hydrothermal	550			N/A	[46]
$Cs_2AgBiBr_6$	Single crystal	1–10 μm	Hydrothermal	650			N/A	[47]
$Cs_2AgBiBr_6$	Film	GS 500 nm	Spin-coating				N/A	[48]
$Cs_2AgBiBr_6$	Single crystal	250 nm	Hydrothermal	440	630	145	N/A	[49]
			Alloyed Perovskites					
$CsSn_{0.5}Ge_{0.5}I_3$	Film	T 200 nm, GS 80 nm	Pyrex tubes annealing	840	830	52	N/A	[56]
$(C_8NH_{12})_4Bi_{0.57}Sb_{0.43}Br_7 \cdot H_2O$	Single crystals	3 mm	Cooling-induced	850	450 and 640		N/A	[52]

* T—film thickness, GS—grain size.

2.1.1. Pb-Substituted Perovskites

• Tin

Sn (II) attracted much attention due to its similarity of the electronic structure with lead atom. Thus, the tin-based perovskites are potentially applicable in the field of optoelectronic devices. In the work [31], a simple and efficient solution-phase method to synthesize Cs_2SnX_6 (X = Br, I) with a good yield, well-defined crystal structure, and long-term stability was demonstrated (Figure 2a,b). Cs_2SnX_6 single crystals show excellent stability against light and moisture due to the unique vacancy-ordered defect-variant structure, stable Sn^{4+} chemical compositions, as well as the lower formation enthalpy for Cs_2SnX_6. Another method [30] is hydrothermal synthesis of $Cs_2SnCl_{6-x}Br_x$ millimeter-size single crystal, with the reaction mixture color continuously changing from transparent to yellow and, finally, to dark red. In addition, the band gap can be changed by the halide composition of single crystals, which leads to continuous tuning of the absorption spectra from near violet to orange spectral region. Also, for these structures, strong surface charge recombination of the excess carriers near the crystal surfaces created by short-wavelength light was observed.

The band gap of tin-based perovskite also can be altered by the changing the chemical composition of A cation. Mixed-cation perovskite system based on the substitution of cesium (Cs+) with rubidium (Rb+) in tin bromide perovskites $Cs_{1-x}Rb_xSnBr_3$, has been experimentally demonstrated in [29]. The pure single-phase samples in compositional range of $CsSnBr_3$–$Cs_{0.70}Rb_{0.30}SnBr_3$ were obtained by high temperature (600 °C) synthesis and all the rubidium-embedding alloys showed a good stability. During chemical substitution from $CsSnBr_3$ to $Cs_{0.70}R_{0.30}SnBr_3$, the crystal lattice passes from cubic to orthorhombic symmetry, which was correlated with optical properties, since the band gap varies from 1.719 to 1.817 eV. To further boost the efficiency and stability of Sn-based perovskite, organic amine salts, such as butylamine (BA), were introduced into the crystal lattice [32]. This method allows more effective control of the crystallization kinetics of low-dimensional Sn perovskite films, due to which these structures acquire improved stability, homogeneity, and oriented crystal growth. Therefore, the crystallization kinetics jointly controlled by Lewis adducts and the ion exchange process using a mixture of ion liquid solvent methylammonium acetate and polar aprotic solvent dimethyl sulfoxide (DMSO) is demonstrated.

• Bismuth

Bi (III) is another non-toxic candidate element for a solution to the toxicity problem of lead-based perovskite materials. Methylammonium bismuth iodide (($MA)_3Bi_2I_9$) is one of most popular lead-free perovskite materials due to its air stability. Since the chemical composition of such a material is similar to organic–inorganic lead halide perovskites, the synthetic routes of film formation developed for lead-based perovskites, such as two-step deposition method, can be adopted for the Bi-based perovskites resulting in controllable morphology and high surface quality. Thus, in the work [39], the formation of $(MA)_3Bi_2I_9$ films was demonstrated. Firstly, BiI_3 was deposited onto the meso-TiO_2 glass substrate followed by the toluene drop-casting and annealing, and secondly, the alcohol solution of MAI was spin coated and heated. For the hole transport layer, spiro-MeOTAD in chlorobenzene was deposited onto the prepared $(MA)_3Bi_2I_9$ films. However, organic–inorganic perovskite films still contain the surface impurities, as pinholes. Wang's group in their work [40] used diethyl ether as anti-solvent to improve the characteristics of $(MA)_3Bi_2I_9$ based films such as compactness and reduce pinhole defects. The $(MA)_3Bi_2I_9$ films treated by diethyl ether were compact with fewer pinholes and devices based on it exposed long-term air stability with 30% humidity for more than 200 days. The morphology of the perovskite film can also be improved by the post-synthetic treatment as was shown in work [36]. Stable $(C_6H_5NH_3)BiI_4$ perovskite film was formed by spin coating followed by the gas pump treatment, which resulted in a dense and pinhole-free film with lateral dimension more than 20 cm^2. This material shows good solubility in ethanol and heat stability confirmed by thermogravimetric analysis. Also due to the presence of a hydrophobic organic chain, it was shown that

the $(C_6H_5NH_3)BiI_4$ perovskite can withstand constant exposure of moisture for one year in ambient. Among the organic–inorganic bismuth-based perovskites, a $(1,3\text{-propanediammonium})_2Bi_2I_{10}\cdot 2H_2O$ with quantum-well morphology can be highlighted [51]. This material has sandwich structure with the inorganic $Bi_2I_{10}^{4-}$ clusters periodically arranged in the crystallographic "c" axis separated by 0.5 nm layers of organic cations. The crystal growth is induced by the slow evaporation of precursors BiI_3 and 1,3-propyl diammonium dihydrogen iodide.

The use of an inorganic cation at the A site of perovskite results in the increased stability and intensity of emission. In the work [38], a synthesis of double-halide single crystal Cs_3BiBr_6 perovskite was shown. The distinctive feature of double-halide perovskite materials is an isolated $BiBr_6$ polyhedron in the crystal lattice. Therefore, the ratio between two raw precursors $BiBr_3$ and CsBr plays key role in controlling the formation of the Cs_3BiBr_6 single crystals. It was also shown that such Cs_3BiBr_6 single crystals with band gap of 2.55 eV possess high thermal stability. To further improve PLQY of $Cs_3Bi_2Br_9$ perovskite NCs, a Eu^{3+}-doping can be used via modified ligand-assisted reprecipitation (LARP) method as was shown in work [53]. The $Cs_3Bi_2Br_9{:}Eu^{3+}$ NCs demonstrate multicolor emissions: Emission from the NC' host $Cs_3Bi_2Br_9$ matrix and the Eu^{3+} ion emissive transition. Compared to the $Cs_3Bi_2Br_9$ NCs, the Eu^{3+}-doped NCs show PLQY more than 40% and moisture stability. Alkali metals such as rubidium (Rb) have a good influence on boosting the optical characteristics of perovskites. Thus, in work [37], $Rb_7Bi_3Cl_{16}$ single crystals with zero-dimensional cluster structure was reported. This structure represents two kinds of octahedra with different distortions. Such NCs were synthesized in a Teflon-lined stainless-steel autoclave, and they emit at 437 nm with a PLQY more than 28%. The moisture-stability of $Rb_7Bi_3Cl_{16}$ NCs was attributed to increased ratio of Rb atoms and the $[BiCl_6]^{3-}$ octahedra on the surface, which formed an inorganic protective BiOCl shell.

- Indium

Another good candidate for lead atom substitution in the perovskite materials is indium. In the work [34], a hydrothermal synthesis of zero-dimensional indium-based $Cs_2InBr_5\cdot H_2O$ single crystal with emission in red spectral region with PLQY of 33% was reported. The strong PL emission is due to self-trapping excitons, which are the result of structural deformation in an excited state. The transition between hydrated $Cs_2InBr_5\cdot H_2O$ and the dehydrated form is accompanied by a switchable double emission, which allows detecting water molecules motion in air or organic solvents (Figure 2c).

- Other elements

Herein, we discuss some nontypical chemical elements that are used in lead-free perovskites. The Pb atom was substituted by Yb in a simple hot-injection synthesis of $CsYbI_3$ NCs with high crystallinity and high uniform size distribution, reported in work [55]. Briefly, during the growth of nanocrystals, Yb (II) was introduced into the cubic ABX_3 perovskite lattice. The synthetic route for formation of the $CsYbI_3$ NCs is similar to that of lead halide perovskites, but with YbI_2 used as a metal halide precursor. The synthesized NCs demonstrated strong excitation-independent emission and high PLQY of 58%. In this work [54], a synthesis of all-inorganic $Cs_3Cu_2I_5$ perovskite crystalline film via a spin-coating method was reported. The $Cs_3Cu_2I_5$ thin film was formed from CsI and CuI precursors sequentially added into a mixed solvent of dimethyl sulfoxide (DMSO) and dimethylformamide (DMF). The perovskite film exhibited pronounced sensitivity to deep UV and UV light illumination with response rise/fall time speeds of 26.2/49.9 ms. Another chemical element that can be used for substitution of lead atom is gold. Two new hybrid organic–inorganic gold perovskite-like halides, $(CH_3NH_3)AuX_4\cdot H_2O$ (X = Br and Cl) were reported in work [50]. Non-stoichiometric 2:1 molar ratio of methylammonium halides (MACl or MABr) and Au (III) halides ($AuBr_3$ or $AuCl_3$) in water/methanol 0.2 M solution system was used. The open flasks with mixture of precursors were kept at room temperature that allowed the evaporation of the solvent. After evaporation, dark red $(CH_3NH_3)AuBr_4\cdot H_2O$ crystals and yellow $(CH_3NH_3)AuCl_4\cdot H_2O$ crystals were obtained with lateral size up to 5 mm. These hydrated crystals formed in a new type structure featuring perovskite-derived

1D chains and 2D layers based on AuX_6 pseudo-octahedral building blocks. At room temperature, both crystals show a weak blue emission, which originates from the electronic transition between Au-6s and Au-5d.
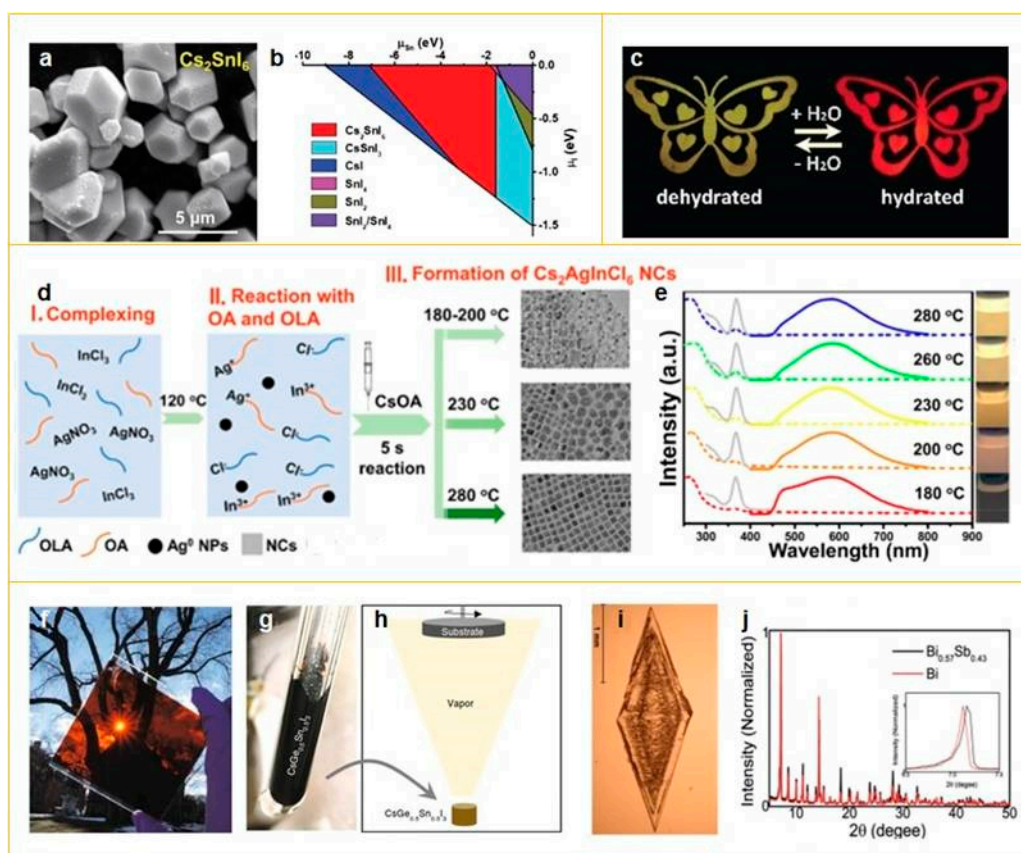

Figure 2. Synthesis of lead-free perovskites. (**a**) SEM images of Cs_2SnI_6; (**b**) calculated phase diagram of Cs–Sn–I. Reproduced with permission [31]. Copyright WILEY-VCH Verlag, GmbH & Co. KGaA, Weinheim, Germany, 2019. (**c**) Visualized dual emission between the hydrated and dehydrated species, fabricated by embedding the perovskite material, $Cs_2InBr_5 \cdot H_2O$ into an etched butterfly pattern. Reproduced with permission [34]. Copyright WILEY-VCH Verlag, GmbH & Co. KGaA, Weinheim, Germany, 2018. (**d**) Schematic representation on the phase formation of $Cs_2AgInCl_6$:Bi NCs at different synthesis temperatures (180–280 °C) in three steps: (I) Complexing of optimized precursors including OA, OlAm, and HCl; (II) $AgNO_3$ and $InCl_3$ reacting with OA to form Ag–oleate and In–oleate and oleylammonium chlorine. Ag^0 NPs are formed by the reduction of Ag+ in the presence of amine ligands; (III) formation of $Cs_2AgInCl_6$ NCs at different synthesis temperatures followed by the injection of CsOA; (**e**) UV–Vis absorption (dashed line), photoluminescence (PL) (excitation at 368 nm), and PL excitation (emission at 580 nm) spectra of Bi-doped $Cs_2AgInCl_6$ NCs dispersion in hexane obtained at different synthesis temperatures (180–280 °C); the insets show the samples irradiated under a 365 nm UV lamp. Reproduced with permission [45]. Copyright American Chemical Society, 2019. (**f**) Photograph of an as-synthesized large-area $CsSn_{0.5}Ge_{0.5}I_3$ perovskite thin film on a glass substrate showing dark reddish color. (**g**) Photograph of as-synthesized $CsSn_{0.5}Ge_{0.5}I_3$ perovskite solid using the melt-crystallization method. (**h**) Schematic illustration of the single-source evaporation method for the deposition of ultrasmooth $CsSn_{0.5}Ge_{0.5}I_3$ perovskite thin film. Reproduced with permission [56] Copyright Springer Nature Limited, 2019. (**i**) Image of $(C_8NH_{12})_4Bi_{0.57}Sb_{0.43}Br_7 \cdot H_2O$ single crystal. (**j**) Powder X-ray diffraction (PXRD) patterns of $(C_8NH_{12})_4Bi_{0.57}Sb_{0.43}Br_7 \cdot H_2O$ (black line) and $(C_8NH_{12})_4BiBr_7 \cdot H_2O$ (red line). Reproduced with permission [52]. Copyright WILEY-VCH Verlag, GmbH & Co. KGaA, Weinheim, Germany, 2019.

2.1.2. Double Perovskites

The other big class of lead-free perovskites is the double perovskites where Pb (II) atom is substituted by pair of Ag (I) and Metal atom of 3+ valence. The most spread chemical composition for lead-free double perovskites is Cs_2AgBiX_6. In the work [44], the dependence of the energetic structure of $Cs_2AgBiBr_6$ thin films on the molar ratio of precursors $CsBr:AgBr:BiBr_3$ was investigated. Precise solution processing allows obtaining accurate composition stoichiometry of $Cs_2AgBiBr_6$ multicomponent perovskite films, and hence good optoelectronic properties. The highly stable $Cs_2AgBiBr_6$ thin film was used as an active material for sensor due to the fact that its electrical properties are significantly dependent on humidity in [48]. Fast response and recovery of this $Cs_2AgBiBr_6$ thin film can be explained by the reversible physical adsorption of water molecules at the surface of thin film. A convenient solution method of synthesis to deposit high-quality $Cs_2AgBiBr_6$ film with long lifetimes, low trap densities, and large grain sizes was developed in work [49]. In this paper, authors optimized the precursor solution using a mixture of DMSO and DMF as the solvents and found that the introduction of a small amount of DMF is helpful to increase the grain size of the obtained $Cs_2AgBiBr_6$ films. As a result, the incorporated excess of DMF may change the ratio of precursors $CsBr:AgBr:BiBr_3$ in the solution and prevent the AgBr to fit within the crystal lattice and to form the impurity in $Cs_3Bi_2Br_9$. However, the use of 10% DMF resulted in formation of double perovskite film and the PL intensity increase with preserved absorption spectrum. This was accompanied with an increase in PL lifetimes, suggesting that reducing the trap densities is consistent with the enlarged grain size and improvement of crystallinity. It was recently shown [47] that these $Cs_2AgBiBr_6$ perovskite materials can be implemented in the photocatalytic system for dye degradation. It was found that during photocatalytic processes, $Cs_2AgBiBr_6$ is stable in ethanol. Acceleration of the reaction between free radicals and dye molecules indicates the unique catalytic properties of the $Cs_2AgBiBr_6$ surface. Also, the deposition of metal clusters, such as Pt onto $Cs_2AgBiBr_6$, effectively enhances the photocatalytic activity.

Along with Bi atoms, Sb and In halides are used in formation of lead-free double perovskites. In work [46], a double $Cs_2AgSbBr_6$ perovskite with an indirect optical bandgap of 1.64 eV was synthesized hydrothermally in aqueous HBr acid. This all-inorganic double $Cs_2AgSbBr_6$ perovskite crystallizes in the cubic space group Fm3m with a = 1.1 nm. After heat treatment at 200 °C, the crystallinity and symmetry were preserved. The atomic ratios of 2.18 (Cs):1.01 (Ag):0.91 (Sb):5.90 (Br) and existence of Sb (V) regions were found, which is consistent with the crystallographic composition and the charge transfer from the Sb (III) to Sb (V). In the work [45], the optimization of the colloidal hot-injection synthesis of undoped and Bi-doped $Cs_2AgInCl_6$ perovskite nanocrystals was described. The whole synthesis conditions such as temperature, number of ligands, and hydrochloric acid were evaluated to enhance the PLQY of Bi-doped $Cs_2AgInCl_6$ NCs (Figure 2d,e). The undoped nanocrystals demonstrated emission at 455 nm and the Bi-doped samples exhibit a broad emission peaked at 580 nm with the PLQY of ~11.4%.

2.1.3. Alloyed Perovskites

Another approach of substitution of Pb atoms in perovskite materials is a formation of alloyed perovskites with mixture of metal atoms at B site in crystal lattice. In the work [56], a synthesis of alloyed cesium tin-germanium triiodide ($CsSn_{0.5}Ge_{0.5}I_3$) perovskite was shown (Figure 2f–h). The perovskite powder with this chemical composition was synthesized by a solid-phase reaction in evacuated Pyrex tubes between mixed $CsI:SnI_2:GeI_2$ solid powder precursors (molar ratio 2:1:1). It was also shown that due to the formation of a stable oxide layer, which fully encapsulated and passivated the perovskite surface, these powders and films exhibited very high stability. The surface-oxide passivation approach reported here represented an alternate way for increasing the stability and efficiency of lead-free perovskites. In the work [52], the synthesis of an air-stable zero-dimensional mixed metal halide $(C_8NH_{12})_4Bi_{0.57}Sb_{0.43}Br_7 \cdot H_2O$ perovskite, in which $[SbBr_6]_3$ and $[BiBr_6]_3$ octahedral units are separated by the organic $C_8H_{12}N^+$ cation, was reported. These single crystals (Figure 2i,j) exhibit moisture and

light stability and show broadband emission ranging from visible to NIR region, which is caused by both free and self-trapped excitons.

2.2. Lead-Free Perovskites Morphology

The analysis of literature shows that lead-free perovskites can be formed as films [32,39,40,44,48,56,57], single crystals [25,26,29,32,33,41,42,44–47,50], and NCs [32,38,40,48,49]. The synthetic methods are similar to that used for lead-based perovskites. Spin-coating of the precursors on the substrates and annealing result in the formation of perovskite films with thickness up to 500 nm and grain size varying from 80 nm to 40 μm. Hydrothermal and induced crystallization methods, including antisolvent diffusion, vapor-assisted, cooling, and slow evaporation, result in the formation of single perovskite crystal with sizes varying from 250 nm to 1–2 cm. LARP and hot injection methods are used for NCs synthesis with diameter up to 10 nm and stabilized by long-chain ligands in non-polar solvents. It is worth mentioning that among the different morphologies of lead-free perovskite materials, the highest PLQY (up to 58% [55]) belongs to NCs, which is of importance for their utilization in lighting applications.

2.3. Stability

Although the lead-free perovskite materials have already found their implementation as an efficient photosensitive media for photodetectors and solar cells [18], these materials are still far from their commercial implementation due to their stability. This drawback becomes crucial when lead-free perovskites are applied as an emissive media in lasing systems and lighting applications. Since almost all chemical properties of lead-free perovskites are similar to that of Pb-based, the methods of stability increasing used for Pb-based can be adopted and implemented for lead-free perovskites. Several methods can be highlighted for this purpose: In-situ synthesis in polar environment [58], in-situ synthesis in protective matrices [59,60], the surface passivation by chemical post-treatment [61,62], and the embedding into the protective matrices [63]. The implementing of the host matrices is most appropriate for the further use in photonics application since this approach allows the in-situ design of the morphology of the active media, including size and shape, which is crucial for the performance of the emitting resonant devices, such as lasers.

Lead-free perovskites already implemented as a photosensitive material for photodetectors [64] and solar cells [18]. In addition, theoretical work [65] predicted that lead-free perovskites have even higher optical absorption compared to lead-based ones, which shows the advantages of their further implementation in all sorts of photovoltaic devices. In the following sections, we will focus on the light-emitting devices and lasers based on lead-free perovskites together with providing the background of the topic.

3. Lighting Applications

The principle of light emission by LED is based on the spontaneous recombination of electron–hole pairs in the active material, which is typically a semiconductor [66]. The radiative recombination can be carried through electroluminescence or photoluminescence. The latter is attributed to the down-conversion LEDs, where the emissive material or phosphor is excited optically by UV or blue chip. Taking into account such outstanding optical properties of perovskite materials as tunable in a wide range PL peak position, high PLQY, and small values of FWHM, there is no doubt that perovskites are promising for utilization as phosphors in LEDs. Indeed, just in the last few years, the luminance and external quantum efficiency of perovskite based LEDs increased their from 364 cd m^{-2} and 0.1% [3] to 76,940 cd m^{-2} and 16.5% [67], respectively. More information on recent developments of lead halide perovskites can be found elsewhere [68–71].

One of the first attempts to minimize the toxicity of lead-based perovskite materials was introducing the mixed-metal cation perovskites, thus decreasing the Pb atoms amount in the active material. In work [72] by Xiaoli Zhang et al., a set of $CsPb_{1-x}Sn_xBr_3$ NCs were synthesized. It was shown that

with increase of Sn content the absorption and emission bands are blue-shifted. The best performance of LED based on mixed-metal cation perovskite material was achieved for Sn content of 0.3 with maximum luminance of 5495 cd m^{-2}.

Recently, an LED based on all-inorganic lead-free film emitter sandwiched between ITO/PEDOT:PSS and TPBi/LiF/Al as the hole and electron injection electrodes, respectively, was demonstrated in work [73] by Anupriya Singh et al. Authors showed that simple spin-coating method can be implemented to synthesize emissive $Cs_3Sb_2X_9$ film, which PL can be tuned via vapor halide exchange method. A visible−infrared radiance of 0.012 W·Sr^{-1}·m^{-2} was achieved at 6 V with $Cs_3Sb_2I_9$ as active layer with electroluminescence peak at 750 nm (Figure 3a,b).

Jiajun Luo et al., at the end of 2018, published work [74] where authors showed that by the modification of the chemical composition of all-inorganic double perovskites, in particular, by alloying Na cations into $Cs_2AgInCl_6$ via hydrothermal method, resulted in suppression the dark transitions. Thus, highly luminescent powders were obtained with PLQY up to 86%. It was shown that optimally alloyed $Cs_2(Ag_{0.60}Na_{0.40})InCl_6$ with 0.04% Bi doping perovskite emits warm-white light with luminance 5000 cd m^{-2} for over 1000 h (Figure 3c,d).

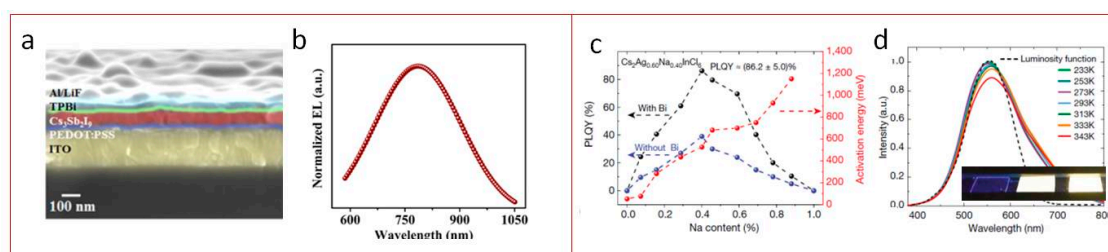**Figure 3.** Lead-free film perovskite-based LEDs. (**a**) Cross-sectional SEM image of device; (**b**) normalized electroluminescence (EL) spectrum of the $Cs_3Sb_2I_9$ film. Reproduced with permission [73]. Copyright American Chemical Society, 2019. (**c**) Activation energy and photoluminescence quantum yields (PLQY) of $Cs_2Ag_xNa_{1-x}InCl_6$ powder vs. Na content. The dashed lines are guides for the eye. (**d**) $Cs_2Ag_{1-x}Na^xInCl_6$ Luminosity function (dashed line) and photoluminescence spectra (solid lines) of $Cs_2Ag_{0.60}Na_{0.40}InCl_6$ measured at different temperatures from 233 K to 343 K. Reproduced with permission [74]. Copyright Springer Nature Limited, 2018.

Besides lead-free films and powders, nanomaterials with perovskite crystal structure also have found their lighting applications. Xiangtong Zhang et al., at the end of 2018, published a letter [75] on lead-free 2D Ruddlesden−Poppertype $(C_{18}H_{35}NH_3)_2SnBr_4$ perovskite with high PLQY up to 88% in solution and 68% in the film. The 2D perovskites were synthesized by a hot injection method and passivated by oleylamine cations. Obtained films were further implemented as active media in the inverted orange LED showing a low turn-on voltage of 2.2 V and a luminance of 350 cd m^{-2} (Figure 4d,e). In 2019, Aifei Wang et al. [76] reported on synthesis of 2D (octylammonium)$_2$SnX$_4$ (X = Br, I) with >80% chemical yield produced by simple heating of the precursors in acid solution in ambient conditions. The synthesized material possesses 600 nm emission with near-unity PLQY. The position of the PL peak can be also tuned by halide exchange. This novel material was further used as a phosphor in down-conversion LED with white light emission (Figure 4a−c).

Zhiwen Yang et al. [77] developed a synthesis of bright blue emissive perovskite NCs inspired by hot injection method [8] with chemical formula CsBr:Eu^{2+} with an FWHM of 31 nm and PLQY of 32.8%. The authors showed principle opportunity to employ these NCs as a phosphor material for fabricating down-conversion white LEDs (Figure 4f,g).
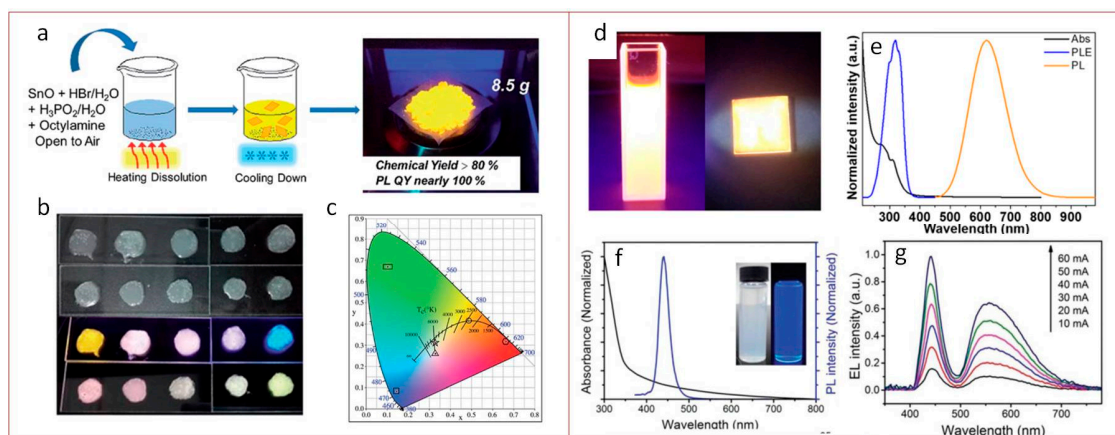
Figure 4. Lead-free perovskite nanomaterials based down-conversion LEDs. (**a**) Schematic representation of the synthesis of the 2D (OCTAm)$_2$SnBr$_4$ by a facile aqueous acid-based synthetic method in ambient air. (**b**) Images of yellow phosphors, blue/green phosphors, and their blends with different ratios embedded in PS films under sunlight (top panel) and 365 nm UV light (bottom panel). The first row in each panel are a yellow–blue phosphor mixture, and the second is a yellow–blue–green mixture. (**c**) Chromaticity coordinates of different ratios of the phosphor mixture plotted on the CIE1931 chromaticity chart: Blue phosphor (square), yellow phosphor (round), yellow–blue phosphor 4:1 (triangle), and yellow–blue–green phosphor 4:1:1.5 (star). Reproduced with permission [76]. Copyright Royal Society of Chemistry, 2019. (**d**) Photograph of the colloidal suspension and film of (OAm)$_2$SnBr$_4$ perovskites under UV light. (**e**) Normalized absorption (Abs), PL excitation (PLE, monitored at 620 nm), and PL (excited by 365 nm) spectra of the (OAm)$_2$SnBr$_4$ perovskite film. Reproduced with permission [75]. Copyright American Chemical Society, 2019. (**f**) Absorption and photoluminescence spectra of CsBr:Eu^{2+} NCs. The inset depicts the optical images of the NCs dispersed in hexane with and without illumination by a 365 nm UV lamp. (**g**) EL spectra and of the white LED operated under different forward bias currents. Reproduced with permission [77]. Copyright WILEY-VCH Verlag, GmbH & Co. KGaA, Weinheim, Germany, 2019.

4. Lasing

The term LASER is the abbreviation for "light amplification by stimulated emission of radiation". Thus, lasers are light-emitting devices via a process of optical amplification based on the stimulated emission in the active (amplifying) medium. The first theoretical prediction of this phenomenon was conducted by Charles Townes and Arthur Schalow [78], which inspired further development of this research field. Since the first laser built by Theodor Maiman in 1960 [79,80], the number of lasers implementing different types of active medium together with the varied resonator's geometries and pump sources significantly increased. These devices found applications in different fields from everyday life, for example CD/DVD to fabrication and scientific tasks such as microscopy with improved spatial resolution [81], etc.

4.1. Basic Principles

The basic and simplified laser configuration consists of the following elements (Figure 5a): (i) An active medium, where the stimulated emission process occurs; (ii) a pump source to produce the population inversion in active media; and (iii) a resonator, which is needed to stimulate the positive feedback mechanism that causes the majority of the atoms to contribute to the coherent output in active medium. The active medium should possess high gain coefficient, which makes possible stimulated emission amplification inside the material (Figure 5b). Briefly, the incoming photon from pump source excites the atom in active medium, and then it undergoes radiative relaxation through either spontaneous emission (SE) or stimulated emission of a coherent photon. The latter interacts with the incident photon from pump source which, in turn, causes the creation of doubled number of coherent

photons. For the normal population of atoms, the SE prevails over the stimulated emission. To obtain the amplification, a population inversion is needed, which can be achieved by pumping the active medium. For that purpose, different sources are implemented so far. All variety of pump sources can be divided into two classes: Optical and electrical pumping. After excitation by pump, source atoms start to emit the photons in all directions and the photons that propagate along the active medium axis can stimulate other excited atoms to emit coherent photons. The "alignment" of emitted photons is achieved by different configurations of the resonators, for instance: (i) Distributed Bragg reflector (DBR), (ii) Fabry–Perot (F-P), (iii) random scattering (or random lasing, RL), and (iv) whispery gallery mode (WGM). The types of resonator's geometry are depicted in Figure 5c.
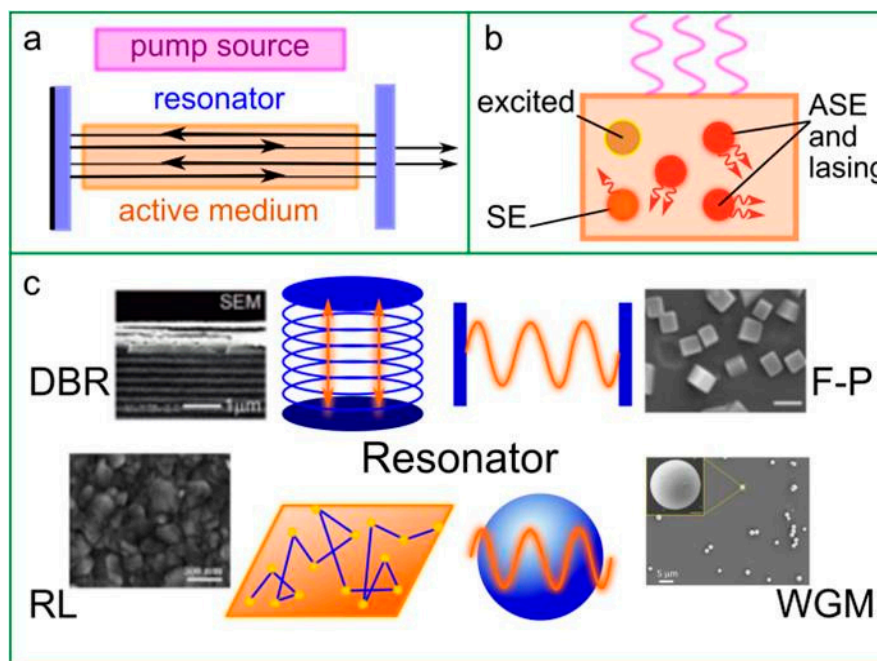

Figure 5. Architecture of perovskite-based lasers. (**a**) Simplified laser configuration. (**b**) Principle of stimulated emission occurred in active media: SE—spontaneous emission, ASE—amplified spontaneous emission. (**c**) Types of resonator's geometries: DBR—distributed Bragg reflector, F-P—Fabry–Perot, RL—random lasing, WGM—whispery gallery mode. Insets in (c) are the examples of the morphology of perovskite materials used for DBR [82], F-P [83], RL [84], and WGM [85] resonators. Adopted with permission [82]. Copyright Royal Society of Chemistry, 2018; Adopted with permission [83]. Copyright American Chemical Society, 2018; Adopted with permission [84]. Copyright American Chemical Society, 2018; Adopted with permission [85]. Copyright Royal Society of Chemistry, 2019.

The simplest resonator is F-P and is formed by two parallel mirrors, one of which is partially transparent (Figure 5a,c). This configuration allows the emitted light to propagate along the axis of amplifying materials, thus resulting in the amplification of the emission. In some cases, the initial reflectivity on the cleaved facets of semiconductor crystal served as active medium at the interface with air is sufficient enough to create a resonator. Most of the lasers based on F-P resonators are multimode. DBR–based resonator consists of multiple layers of materials with different refractive index (Figure 5c). On boundary between the layers, a constructive interference for waves with specific wavelength can occur. The efficiency of reflectance of a light emitted by an active medium in DBR resonator reaches 99%, thus this type of resonator is highly utilized in different laser systems such as vertical-cavity surface-emitting lasers (VCSELs) where quantum wells or thin films of luminescent material are used as active medium. WGM-based resonator is formed by a concave surface where a total optical internal reflection occurs for specific waves (Figure 5c). Thus, a light propagates inside the spherical cavity and amplifies by the interaction with the excited atoms in active medium. RL is not a resonator itself since

the optical feedback in this case is provided by scattering particles in active medium, which can also emit light (Figure 5c). However, it is applicable for nanostructured materials with variable reflective index within material volume, for instance, for ensembles of QDs with high PLQY.

4.2. Perovskite Materials in Lasers

To the best of our knowledge, the first observation of the lasing in perovskite materials is dated 1997 [86]. Takashi Kondo et al. reported on lasing of two-dimensional $(C_6H_{13}NH_3)_2PbI_4$ perovskite thin film, which was achieved at 16 K and at 20 kW/cm^2 laser pumping threshold. The main burst in this scientific area of utilizing the perovskite materials in lightning and lasing applications was caused by the synthesis of highly luminescent perovskite materials with QY above 80% [61,87]. At the present moment, the lasing perovskite materials possess wide range of morphology, including thin films [82,84,88–92], microstructures such as cubes [83,93–97], plates [81,98–100], wires [99,101–104], spheres [85,95,105], pyramids [97], nanosheets [106,107], microdisks [108,109], and quantum confined materials such as 2D R-P [110–113] and NCs [114–117], including NCs in glasses [118] and polymers [119]. Also, for the enhancement of the device performance, the perovskite materials can be patterned by ion beam lithography [109], laser ablation [108], or imprinting methods [89,120], and can be applied on the initially patterned substrates [81,90]. Perovskite-based lasers usually are optically pumped, which can be also up-conversion excitation of PL [83,84,92,96,106,116,118]. By the type of pump source operation, one can consider pulsed [57,82,92,109,112,113] and continuous wave (CW) [89,102,119,121] light sources used. The electrical type of pumping [122] is not so widely used, however, is still perspective. As in the case of conventional lasers, perovskite-based lasers are also formed with resonators such as DBR or waveguide [82,89–91,110,113,114,119,120] and F-P [94,97,101–104,114,123] (Figure 6), and WGM [57,85,93,95,96,99,100,105–109,115,124] and RL [84,88,92,111,112,116–118] (Figure 7).
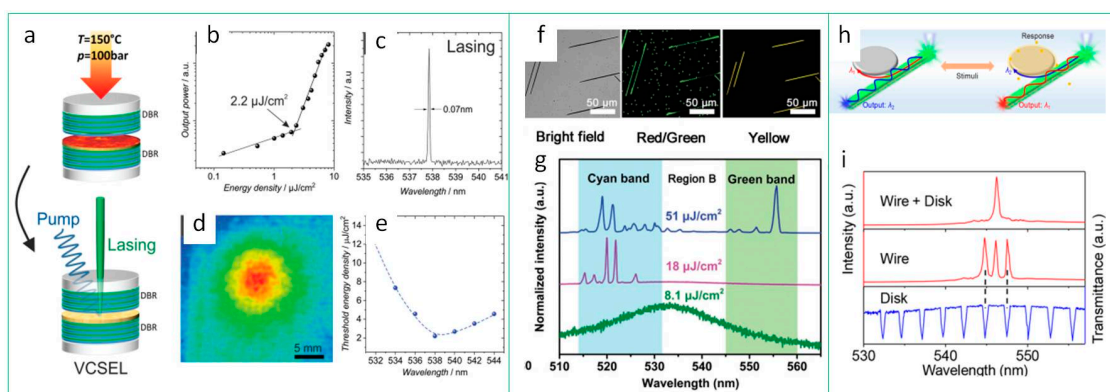

Figure 6. Resonators vs. perovskite material's morphology. DBR: (**a**) Scheme of vertical-cavity surface-emitting lasers (VCSEL) device; (**b**) output power vs. pump energy density; (**c**) PL spectrum and (**d**) far-field beam distribution at pump energy density above threshold; (**e**) energy density of laser threshold energy vs. the PL peak position. Reproduced with permission [120]. Copyright WILEY-VCH Verlag, GmbH & Co. KGaA, Weinheim, Germany, 2019. F-P: (**f**) Microimages (bright field, green channel, yellow channel); (**g**) pump fluence dependent PL spectra of central region of CsPbBr$_x$I$_{3−x}$ nanowires. Reproduced with permission [125]. Copyright WILEY-VCH Verlag, GmbH & Co. KGaA, Weinheim, Germany, 2018. F-P combined with WGM disk: (**h**) Scheme of the switchable single-mode lasing from a perovskite microwire coupled with an organic microdisk; (**i**) transition from multimode to single-mode lasing of the typical MAPbBr$_3$ nanowire coupled with a microdisk. Reproduced with permission [103]. Copyright American Chemical Society, 2018.
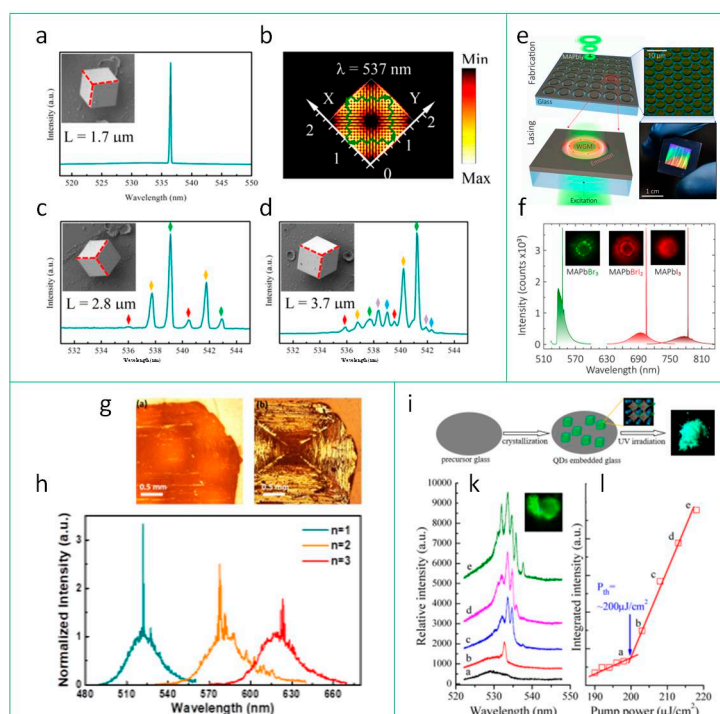
Figure 7. Resonators vs. perovskite material's morphology. WGM: (**a**,**c**,**d**) lasing spectra of the $CsPbBr_3$ microcuboids of different size, the insets are corresponding SEM images of the samples; (**b**) numerical simulations on the standing wave field distributions, which are confined in the square cross-section of cube with size of 1.7 μm. Reproduced with permission [96]. Copyright American Chemical Society, 2019. Array of WGM resonators: (**e**) Scheme of microlasers array fabrication, false-color SEM image, and a photo of a 1×1 cm^2 array; (**f**) lasing spectra from perovskite microlasers from $MAPbI_3$ (brown curve), $MAPbBrI_2$ (red curve), and $MAPbBr_3$ (green curve), the insets are PL images of the samples. Reproduced with permission [108]. Copyright American Chemical Society, 2019. RL: (**g**) Optical images of the $(BA)_2PbI_4$ (n = 1) single crystal bottom and top surface; (**h**) lasing spectra from high-quality homologous 2D perovskite single crystals with n = 1, 2, 3. Reproduced with permission [111]. Copyright American Chemical Society, 2018. (**i**) Scheme of a fabrication $CsPbBr_3$ QD-embedded glass (QDs@glass) via in-situ crystallization; (**k**) up-conversion PL spectra of QDs@glass vs. the pump power of 800 nm laser, the inset is a photo of sample excited with energy density above threshold; (**l**) PL intensity vs. pump energy density. Reproduced with permission [118]. Copyright American Chemical Society, 2018.

From the analysis of recent publications, it can be inferred that the active material and corresponding type of resonator are connected to each other. DBR or VCSEL are suitable for the perovskite thin films, which can be easily deposited on the mirrors or waveguide surfaces via CVD or "wet" precursor spin-casting routes. In work [120], it was shown that the room temperature lasing can be achieved in $CsPbBr_3$ thermally imprinted layers as active material at threshold down to 2.2 μJ cm^{-2} (Figure 6a–e). The single crystals, which are grown from the precursor solution on the substrates, can play role of the microcavity themselves. For instance, the perovskite microwires serve as the active medium and F-P resonator at the same time. In work [125], it was shown that composition-graded $CsPbBr_xI_{3-x}$ nanowires can be formed by vapor-phase growth on mica, which possess varied bandgaps along the wire and, hence, blueshifted emission observed at the wire's ends (Figure 6f). In these wires, a double-color lasing is achieved with 35 nm separation between the emission bands, shown in Figure 6g. Since the F-P resonators provide a multi-mode generation, a controllable selection of lasing mode is in high demand for future tunable lasers. In work [103], the authors showed the implementation of organic microdisk with specific transmittance spectrum, which can be used as a filter for the lasing modes of perovskite microwires, as shown in Figure 6h,i.

By altering the shape of micro-sized perovskite materials, an emission enhancement by WGM can be achieved. Thus, WG modes are observed in microspheres, microcubes, microdisks, etc. (Figure 7a–f). In work [96], it was shown that by varying the length of the perovskite cuboid edge, a single- to multi-mode upconversion lasing is obtained at room temperature, which is also confirmed by numerical calculations of standing wave field distribution inside the perovskite cavity (Figure 7b). Thus, wavelength of lasing can be tuned from 534 to 544 nm via the size of the cavity (Figure 7a,c,d). In work [108], it was shown that the single mode lasing in the centimeter-sized arrays of perovskite microdisks can be achieved by the pattering the thin film via laser ablation (Figure 5e). Since the morphology of microdisks can be easily changed, it makes it possible to controllably tune the operating wavelength in the range from 550 to 800 nm (Figure 7f).

As for the conventional amplifying materials, the random lasing occurs in perovskite thin films with grain morphology, layered (R-P type) perovskites structure, or in ensembles of perovskite NCs, where the light is efficiently scattered on the structure boundaries. In work [111], it was shown that in 2D hybrid perovskite single crystals grown by slow evaporation method, a lasing is observed at room temperature (Figure 7g). The lasing wavelength can be tuned from 520 to 625 nm by engineering the perovskite layer thickness from one layer to three layers, respectively (Figure 7h). In work [118], it was shown that TeO_2-based glass matrix with in situ synthesized $CsPbBr_3$ NCs is a good candidate for implementing as an active medium in lightning devices (Figure 7i). Besides the photostability, moisture resistance, and thermal stability of such material, the RL were observed at room temperature pumped with relatively low threshold (Figure 7k,l).

The information from the publications starting from 2017 is summarized in Table 2 where the champion devices are shown. The analysis showed that the highest quality values, Q, are achieved for the single crystal perovskite microcavities with WGM resonator type. In [96], a Q = 10,100 was achieved in all-inorganic $CsPbBr_3$ microcuboids with emission in green spectral region. The second efficient resonator in a frame of the highest Q value is VCSEL for which Q = 5400 was registered with $CsPbX_3$ thin films used as active medium [120]. For lasers implementing F-P type resonators, the maximal Q value of 2500 was achieved for $MAPbBr_3$ microcrystals [81]. For the RL case, the highest Q value of 1040 was registered for 2D R-P layers [111]. Thus, the synthetic routes, which determine the morphology of the nanostructured perovskite materials, also affect the type of a laser.

Lead-Free Perovskite for Lasing

Since the amplification of the stimulated emission imposes high demands on the active medium, lead-free perovskites are still not widely implemented in lasing systems. In 2016, Guichuan Xing et al. published their work [126] on NIR lasing from tin-based perovskite. They showed that tin-based halide perovskites ($CsSnX_3$, X = Br, I) surprisingly possess exceptional optical gain properties in the near-infrared region up to ≈1 μm, which cannot be achieved with lead-based perovskites. NIR lasing with Q ≈ 500 is achieved using the natural photonic crystal at ultralow-threshold (≈6 μJ cm^{-2}) from 20% SnF_2-added to $CsSnI_3$ samples, which are comparable to their lead-based counterparts (Figure 8a–e). This work confirmed the possibility of lead-free perovskites implementation in the lightning and lasing application despite poor photovoltaic performance.
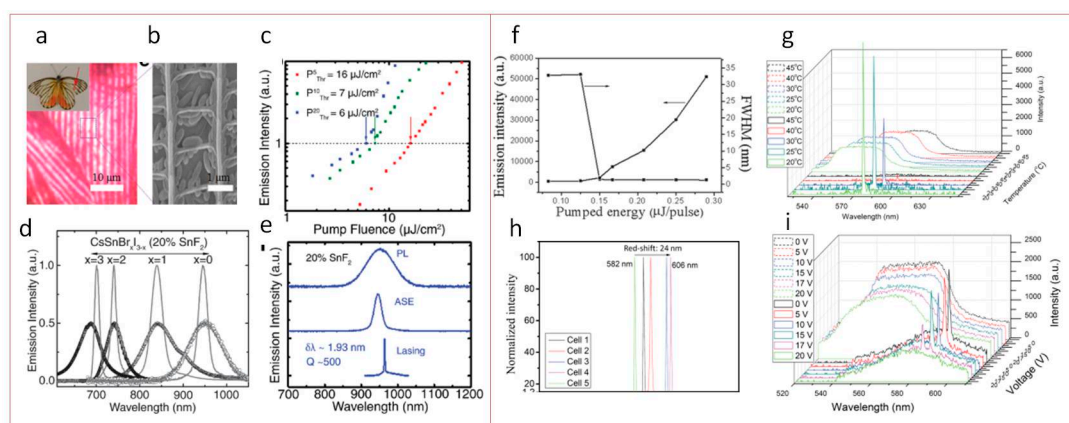
Figure 8. Lasing in lead-free perovskite materials. (**a**) Optical image of a butterfly scale from the white part of the wing. Inset is a photograph of the butterfly. (**b**) SEM image showing lamellae (vertical structures) in the scale. (**c**) Variable fluence measurements reveal the amplified spontaneous emission (ASE) thresholds of the SnF_2-treated samples. (**d**) Wide PL and ASE wavelength tunability from $CsSnBr_xI_{3-x}$ films fabricated by facile mixing the precursor solutions under 500 nm pump pulses (50 fs, 1 kHz). (**e**) A comparison of the PL, ASE, and single-mode lasing of $CsSnI_3$ (20% SnF_2) under 650 nm pump pulses (50 fs, 1 kHz). Reproduced with permission [126]. Copyright WILEY-VCH Verlag, GmbH & Co. KGaA, Weinheim, Germany, 2016. (**f**) Variation in PL intensity and FWHM with pumped energy. (**g**) Thermal tunability of the AIPQD−CLC laser at E = 5.0 μJ/pulse at 20, 25, 30, 40, and 45 °C. (**h**) Tuning of the lasing emission of AIPQD−CLC laser by changing the chiral dopant content in the CLC. (**i**) Electrical tunability of the AIPQD−CLC laser at E = 4.0 μJ/pulse under AC voltages of 0−20 V (1 kHz). Reproduced with permission [127]. Copyright American Chemical Society, 2018.

In the work [127] by Lin-Jer Chen, a performance of laser based on cholesteric liquid crystal (CLC) doped with $CsSnI_3$ QDs (AIPQD−CLC laser) with highly spectral tunability and long-term stability was demonstrated. The $CsSnI_3$ QDs were obtained through a low-cost solvothermal pretreatment process with PL peak at 594 nm with FWHM of 35 nm. Under the optical pump with energy of 0.15 μJ/pulse, FWHM of PL peak decreased down to 0.20 nm with significant PL intensity increase (Figure 8f). These parameters are comparable to those of traditional dye-doped CLC lasers. It was shown that the laser based on lead-free perovskite QDs possessed high stability during storage in ambient (room temperature and humidity of 60%) and retained ~87% of its initial lasing efficiency after half a year. One of the interesting findings is that the lasing wavelength can be tuned by various approaches: Modification of the ratio of the chiral dopant in liquid crystal, changing the temperature, or applying different alternating current (AC) voltages to the active media in the laser (Figure 8g–i).

Table 2. Lasing parameters (type of resonator, pump source, lasing threshold, Q) vs. type of perovskite material (chemical formula, morphology, emission parameters) for the samples with the best performance.

Chemical Formula	Type of Perovskite	Type of Resonator	Pump Source	Lasing Threshold (CW—kW/cm²; P—μJ/cm²)	Spontaneous Emission		Stimulated Emission		Q max	Ref.
					PL Peak, nm; PLQY	FWHM, nm	PL Peak, nm	FWHM, nm		
$(C_6H_{13}NH_3)_2PbI_4$	thin film	DBR	337 nm, 3 ns	20 @ 16 K	543	N/A	544	2	272	[86]
$MAPbI_3$	nanoimprinted thin film	DFB	CW 355 nm	$13 \cdot 10^{-3}$	780	N/A	780	1.16	672	[89]
$MAPbI_3$	thin film on the grating	DFB	532 nm, 1 ns	235	780	50	784	0.4	1960	[90]
$MAPbX_3$	NCs	DFB	CW 405 nm	15–$58 \cdot 10^{-3}$	515/540; 95–97%	30	538.7	0.45	1200	[119]
$CsPbX_3$	thin films	VCSEL	355 nm, 0.3 ns, 1 kHz	2.2	538; 68%	20	538.3	0.07	5400	[120]
$MAPbBr_3$	microcrystals	F-P	400 nm, 100 fs, 1 kHz	9.1	530	40	548	0.21	2500	[81]
$CsPbBr_3$	nanocuboid	F-P	400/800 nm, 35 fs, 1k Hz	40.2	530	18	539.2	0.29	2075/1859	[83]
$CsPbBr_3$	nanowires	F-P	CW 450 nm	6 @ 77 K	530	15	533	0.25	2300	[102]
$(OA)_2(MA)_{n-1}Pb_nBr_{3n+1}$	2D R–P layers	F-P	400 nm, fs	8	530; 65%	30	545	0.3–0.6	1815	[123]
$CsPbBr_3$	microcuboids	WGM	400 nm, 40 fs, 10 kHz	16.9	525	15.6	540.9	0.064	8500	[95]
$CsPbBr_3$	microcuboids	WGM	800 nm, 40 fs, 10 kHz	210	528	20	536.8	0.053	10,100	[96]
$CsPbBr_3$	microspheres	WGM	800 nm, 120 fs, 76 MHz	3.5 @ 300 K 0.4 @ 77 K	530	20	535–540	0.15	3600	[85]
$(C_4H_9NH_3)_2(CH_3NH_3)_{n-1}Pb_nI_{3n+1}$ (n = 1, 2, and 3)	2D R–P layers	RL	374 nm, 55 ps, 40 MHz	2.85	520–630	20	520–630	<0.5	1040	[111]
$(BA)_2(MA)_{n-1}Pb_nI_{3n+1}$	2D layers	RL	400 nm, 80 fs, 1 kHz	2.3 @ 70 K	520–680	15	520–680	0.9	755	[112]
$MAPbBr_3$	thin films	RL	800/400 nm, 35 fs, 1 kHz	0.15 @ 300 K	535/545	30	550	5	110	[92]
$CsSnX_3$ (X = Br, I) doped with SnF_2	Film	DFB	650 nm, 50 fs, 1 kHz	6	680–950; 13%	50–100	950	1.93	500	[126]
$CsSnI_3$	NCs in CLCC	DFB	532 nm, 8 ns, 10 Hz	800	594	35	579–606	0.2	2895	[127]

5. Outline and Perspectives

In the present mini-review, we briefly analyzed the state of art in the field of R&D of organic-inorganic and all-inorganic lead-free perovskites as crystal materials of different dimensionality with improved functional (detection and emission) properties for modern nanophotonics and photovoltaics. The main attention was paid to the recent publications on the development of active media based on lead-free perovskite materials for light sources demonstrating stimulated emission (lasing). The choice and design of laser resonators, influence of morphology of the perovskite active media, and methods for tuning the wavelength of laser emission were discussed. The almost 100% emission QY, possibility to change the lasing wavelength by changing the perovskite chemical composition and morphology, as well as by choice of type and design of resonators make perovskite-based active media very attractive for implementing in laser and lighting sources. It is important to mention that synthetic routes and device fabrication previously developed for lead-based perovskite materials can be efficiently inherent and adopted for their lead-free relatives, hence paving the way to perovskite "green" photonics. Although the number of scientific papers devoted to lead-free perovskite materials have increased in the past few years, there is still plenty of room for further development and improvement of their optical and electronic properties. According to the literature, at least 600 lead-free compounds with double perovskite crystal structure have not been investigated yet [16]. Along with the variety of chemical composition of lead-free perovskite materials, the chemical approaches of their synthesis and passivation are still unexplored. Thus, we highlight perspectives in the field of lead-free perovskites for lighting applications:

- Chemical composition and morphology. To date, Bi-based perovskite materials provide a wide variety of morphology of materials with perovskite symmetry, including double perovskites, along with the excellent and stable performance. The other direction is the search of novel chemical compounds for substituting the lead atom in lanthanide series, such as Yb;

- Synthetic approaches. Inspired by the chemical routes implemented for lead-based perovskites, the vapor deposition approaches might be admitted as synthesis route for formation micrometer-sized lead-free perovskites, the shape of which can meet the resonance conditions for stimulated amplification of the emission;

- Active medium protection. The use of the matrices for in-situ synthesis or as host matrices for perovskite materials can expand the variety of chemical compounds used, i.e., unstable in ambient, together with simple control of the architecture of the active medium defined by matrix morphology.

Thus, lead-free perovskite materials as elements of "green" technology are expected to be intensively studied and further applied in the light emitting devices in nearest future.

Conflicts of Interest: The authors declare no conflict of interest.

References

1. Radhakrishna, S. Polarised luminescence from lead centers in cesium halides. *J. Lumin.* **1976**, *12–13*, 409–411. [CrossRef]

2. Mitzi, D.B. *Synthesis, Structure, and Properties of Organic-Inorganic Perovskites and Related Materials*; John Wiley & Sons, Inc.: New York, NY, USA, 1999; Volume 48, ISBN 9780470166499.

3. Tan, Z.K.; Moghaddam, R.S.; Lai, M.L.; Docampo, P.; Higler, R.; Deschler, F.; Price, M.; Sadhanala, A.; Pazos, L.M.; Credgington, D.; et al. Bright light-emitting diodes based on organometal halide perovskite. *Nat. Nanotechnol.* **2014**, *9*, 687–692. [CrossRef] [PubMed]

4. Stranks, S.D.; Eperon, G.E.; Grancini, G.; Menelaou, C.; Alcocer, M.J.P.; Leijtens, T.; Herz, L.M.; Petrozza, A.; Snaith, H.J. Electron-hole diffusion lengths exceeding 1 micrometer in an organometal trihalide perovskite absorber. *Science* **2013**, *342*, 341–344. [CrossRef] [PubMed]

5. Tyagi, P.; Arveson, S.M.; Tisdale, W.A. Colloidal Organohalide Perovskite Nanoplatelets Exhibiting Quantum Confinement. *J. Phys. Chem. Lett.* **2015**, *6*, 1911–1916. [CrossRef] [PubMed]

6. Sichert, J.A.; Tong, Y.; Mutz, N.; Vollmer, M.; Fischer, S.; Milowska, K.Z.; García Cortadella, R.; Nickel, B.; Cardenas-Daw, C.; Stolarczyk, J.K.; et al. Quantum Size Effect in Organometal Halide Perovskite Nanoplatelets. *Nano Lett.* **2015**, *15*, 6521–6527. [CrossRef]

7. Schmidt, L.C.; Pertegás, A.; González-Carrero, S.; Malinkiewicz, O.; Agouram, S.; Mínguez Espallargas, G.; Bolink, H.J.; Galian, R.E.; Pérez-Prieto, J. Nontemplate synthesis of CH3NH3PbBr3 perovskite nanoparticles. *J. Am. Chem. Soc.* **2014**, *136*, 850–853. [CrossRef]

8. Protesescu, L.; Yakunin, S.; Bodnarchuk, M.I.; Krieg, F.; Caputo, R.; Hendon, C.H.; Yang, R.X.; Walsh, A.; Kovalenko, M.V. Nanocrystals of Cesium Lead Halide Perovskites (CsPbX3, X = Cl, Br, and I): Novel Optoelectronic Materials Showing Bright Emission with Wide Color Gamut. *Nano Lett.* **2015**, *15*, 3692–3696. [CrossRef]

9. Ha, S.T.; Su, R.; Xing, J.; Zhang, Q.; Xiong, Q. Metal halide perovskite nanomaterials: Synthesis and applications. *Chem. Sci.* **2017**, *8*, 2522–2536. [CrossRef]

10. Akkerman, Q.A.; Rainò, G.; Kovalenko, M.V.; Manna, L. Genesis, challenges and opportunities for colloidal lead halide perovskite nanocrystals. *Nat. Mater.* **2018**, *17*, 394. [CrossRef]

11. Weidman, M.C.; Goodman, A.J.; Tisdale, W.A. Colloidal Halide Perovskite Nanoplatelets: An Exciting New Class of Semiconductor Nanomaterials. *Chem. Mater.* **2017**, *29*, 5019–5030. [CrossRef]

12. Shi, E.; Gao, Y.; Finkenauer, B.P.; Akriti, A.; Coffey, A.H.; Dou, L. Two-dimensional halide perovskite nanomaterials and heterostructures. *Chem. Soc. Rev.* **2018**, *47*, 6046–6072. [CrossRef] [PubMed]

13. Smith, M.D.; Connor, B.A.; Karunadasa, H.I. Tuning the Luminescence of Layered Halide Perovskites. *Chem. Rev.* **2019**, *119*, 3104–3139. [CrossRef] [PubMed]

14. Jena, A.K.; Kulkarni, A.; Miyasaka, T. Halide Perovskite Photovoltaics: Background, Status, and Future Prospects. *Chem. Rev.* **2019**, *119*, 3036–3103. [CrossRef] [PubMed]

15. Schulz, P.; Cahen, D.; Kahn, A. Halide Perovskites: Is It All about the Interfaces? *Chem. Rev.* **2019**, *119*, 3349–3417. [CrossRef]

16. Shamsi, J.; Urban, A.S.; Imran, M.; De Trizio, L.; Manna, L. Metal Halide Perovskite Nanocrystals: Synthesis, Post-Synthesis Modifications, and Their Optical Properties. *Chem. Rev.* **2019**, *119*, 3296–3348. [CrossRef]

17. Shi, Z.; Guo, J.; Chen, Y.; Li, Q.; Pan, Y.; Zhang, H.; Xia, Y.; Huang, W. Lead-Free Organic–Inorganic Hybrid Perovskites for Photovoltaic Applications: Recent Advances and Perspectives. *Adv. Mater.* **2017**, *29*, 1605005. [CrossRef]

18. Sani, F.; Shafie, S.; Lim, H.N.; Musa, A.O. Advancement on lead-free organic-inorganic halide perovskite solar cells: A review. *Materials* **2018**, *11*, 1008. [CrossRef]

19. Sun, J.; Yang, J.; Lee, J.I.; Cho, J.H.; Kang, M.S. Lead-Free Perovskite Nanocrystals for Light-Emitting Devices. *J. Phys. Chem. Lett.* **2018**, *9*, 1573–1583. [CrossRef]

20. Luo, J.; Hu, M.; Niu, G.; Tang, J. Lead-Free Halide Perovskites and Perovskite Variants as Phosphors toward Light-Emitting Applications. *ACS Appl. Mater. Interfaces* **2019**, *11*, 31575–31584. [CrossRef]

21. Wang, J.; Dong, J.; Lu, F.; Sun, C.; Zhang, Q.; Wang, N. Two-dimensional lead-free halide perovskite materials and devices. *J. Mater. Chem. A* **2019**, *7*, 23563–23576. [CrossRef]

22. Stylianakis, M.M.; Maksudov, T.; Panagiotopoulos, A.; Kakavelakis, G.; Petridis, K. Inorganic and Hybrid Perovskite Based Laser Devices: A Review. *Materials* **2019**, *12*, 859. [CrossRef] [PubMed]

23. Giorgi, M.; Anni, M. Amplified Spontaneous Emission and Lasing in Lead Halide Perovskites: State of the Art and Perspectives. *Appl. Sci.* **2019**, *9*, 4591. [CrossRef]

24. Ling, Y.; Tian, Y.; Wang, X.; Wang, J.C.; Knox, J.M.; Perez-Orive, F.; Du, Y.; Tan, L.; Hanson, K.; Ma, B.; et al. Enhanced Optical and Electrical Properties of Polymer-Assisted All-Inorganic Perovskites for Light-Emitting Diodes. *Adv. Mater.* **2016**, *28*, 8983–8989. [CrossRef] [PubMed]

25. Liang, D.; Peng, Y.; Fu, Y.; Shearer, M.J.; Zhang, J.; Zhai, J.; Zhang, Y.; Hamers, R.J.; Andrew, T.L.; Jin, S. Color-Pure Violet-Light-Emitting Diodes Based on Layered Lead Halide Perovskite Nanoplates. *ACS Nano* **2016**, *10*, 6897–6904. [CrossRef]

26. Mondal, N.; De, A.; Samanta, A. Achieving Near-Unity Photoluminescence Efficiency for Blue-Violet-Emitting Perovskite Nanocrystals. *ACS Energy Lett.* **2019**, *4*, 32–39. [CrossRef]

27. Gonzalez-Carrero, S.; Francés-Soriano, L.; González-Béjar, M.; Agouram, S.; Galian, R.E.; Pérez-Prieto, J. The Luminescence of CH3NH3PbBr3 Perovskite Nanoparticles Crests the Summit and Their Photostability under Wet Conditions is Enhanced. *Small* **2016**, *12*, 5245–5250. [CrossRef]

28. Wang, N.; Zhou, Y.; Ju, M.-G.; Garces, H.F.; Ding, T.; Pang, S.; Zeng, X.C.; Padture, N.P.; Sun, X.W. Heterojunction-Depleted Lead-Free Perovskite Solar Cells with Coarse-Grained B-γ-CsSnI3 Thin Films. *Adv. Energy Mater.* **2016**, *6*, 1601130. [CrossRef]

29. Bernasconi, A.; Rizzo, A.; Listorti, A.; Mahata, A.; Mosconi, E.; De Angelis, F.; Malavasi, L. Synthesis, Properties, and Modeling of Cs 1-x Rb x SnBr 3 Solid Solution: A New Mixed-Cation Lead-Free All-Inorganic Perovskite System. *Chem. Mater.* **2019**, *31*, 3527–3533. [CrossRef]

30. Zhou, J.; Luo, J.; Rong, X.; Wei, P.; Molokeev, M.S.; Huang, Y.; Zhao, J.; Liu, Q.; Zhang, X.; Tang, J.; et al. Lead-Free Perovskite Derivative Cs2SnCl6−xBrx Single Crystals for Narrowband Photodetectors. *Adv. Opt. Mater.* **2019**, *7*, 1900139. [CrossRef]

31. Han, X.; Liang, J.; Yang, J.-H.; Soni, K.; Fang, Q.; Wang, W.; Zhang, J.; Jia, S.; Martí, A.A.; Zhao, Y.; et al. Lead-Free Double Perovskite Cs2SnX6: Facile Solution Synthesis and Excellent Stability. *Small* **2019**, *15*, 1901650. [CrossRef]

32. Qiu, J.; Xia, Y.; Chen, Y.; Huang, W. Management of Crystallization Kinetics for Efficient and Stable Low-Dimensional Ruddlesden–Popper (LDRP) Lead-Free Perovskite Solar Cells. *Adv. Sci.* **2019**, *6*, 1800793. [CrossRef] [PubMed]

33. Kerner, R.A.; Rand, B.P. Electrochemical and Thermal Etching of Indium Tin Oxide by Solid-State Hybrid Organic–Inorganic Perovskites. *ACS Appl. Energy Mater.* **2019**, *2*, 6097–6101. [CrossRef]

34. Zhou, L.; Liao, J.-F.; Huang, Z.-G.; Wei, J.-H.; Wang, X.-D.; Li, W.-G.; Chen, H.-Y.; Kuang, D.-B.; Su, C.-Y. A Highly Red-Emissive Lead-Free Indium-Based Perovskite Single Crystal for Sensitive Water Detection. *Angew. Chem. Int. Ed.* **2019**, *58*, 5277–5281. [CrossRef] [PubMed]

35. Zhang, Z.; Li, X.; Xia, X.; Wang, Z.; Huang, Z.; Lei, B.; Gao, Y. High-Quality (CH3NH3)3Bi2I9 Film-Based Solar Cells: Pushing Efficiency up to 1.64%. *J. Phys. Chem. Lett.* **2017**, *8*, 4300–4307. [CrossRef] [PubMed]

36. Li, X.-L.; Gao, L.-L.; Ding, B.; Chu, Q.-Q.; Li, Z.; Yang, G.-J. (C6H5NH3)BiI4: A lead-free perovskite with >330 days humidity stability for optoelectronic applications. *J. Mater. Chem. A* **2019**, *7*, 15722–15730. [CrossRef]

37. Xie, J.-L.; Huang, Z.-Q.; Wang, B.; Chen, W.-J.; Lu, W.-X.; Liu, X.; Song, J.-L. New lead-free perovskite Rb7Bi3Cl16 nanocrystals with blue luminescence and excellent moisture-stability. *Nanoscale* **2019**, *11*, 6719–6726. [CrossRef] [PubMed]

38. Tang, Y.; Liang, M.; Chang, B.; Sun, H.; Zheng, K.; Pullerits, T.; Chi, Q. Lead-free double halide perovskite Cs3BiBr6 with well-defined crystal structure and high thermal stability for optoelectronics. *J. Mater. Chem. C* **2019**, *7*, 3369–3374. [CrossRef]

39. Ahmad, K.; Ansari, S.N.; Natarajan, K.; Mobin, S.M. A (CH3NH3)3Bi2I9 Perovskite Based on a Two-Step Deposition Method: Lead-Free, Highly Stable, and with Enhanced Photovoltaic Performance. *ChemElectroChem* **2019**, *6*, 1192–1198. [CrossRef]

40. Liu, Z.; Chen, M.; Wan, L.; Liu, Y.; Wang, Y.; Gan, Y.; Guo, Z.; Eder, D.; Wang, S. Anti-solvent spin-coating for improving morphology of lead-free (CH3NH3)3Bi2I9 perovskite films. *SN Appl. Sci.* **2019**, *1*, 706. [CrossRef]

41. Zuo, C.; Ding, L. Lead-free Perovskite Materials (NH4)3Sb2IxBr9−x. *Angew. Chem. Int. Ed.* **2017**, *56*, 6528–6532. [CrossRef]

42. Du, K.Z.; Meng, W.; Wang, X.; Yan, Y.; Mitzi, D.B. Bandgap Engineering of Lead-Free Double Perovskite Cs2AgBiBr6 through Trivalent Metal Alloying. *Angew. Chem. Int. Ed.* **2017**, *56*, 8158–8162. [CrossRef] [PubMed]

43. Dahl, J.C.; Osowiecki, W.T.; Cai, Y.; Swabeck, J.K.; Bekenstein, Y.; Asta, M.; Chan, E.M.; Alivisatos, A.P. Probing the Stability and Band Gaps of Cs2AgInCl6 and Cs2AgSbCl6 Lead-Free Double Perovskite Nanocrystals. *Chem. Mater.* **2019**, *31*, 3134–3143. [CrossRef]

44. Igbari, F.; Wang, R.; Wang, Z.-K.; Ma, X.-J.; Wang, Q.; Wang, K.-L.; Zhang, Y.; Liao, L.-S.; Yang, Y. Composition Stoichiometry of Cs2AgBiBr6 Films for Highly Efficient Lead-Free Perovskite Solar Cells. *Nano Lett.* **2019**, *19*, 2066–2073. [CrossRef] [PubMed]

45. Liu, Y.; Jing, Y.; Zhao, J.; Liu, Q.; Xia, Z. Design Optimization of Lead-Free Perovskite Cs2AgInCl6:Bi Nanocrystals with 11.4% Photoluminescence Quantum Yield. *Chem. Mater.* **2019**, *31*, 3333–3339. [CrossRef]

46. Wei, F.; Deng, Z.; Sun, S.; Hartono, N.T.P.; Seng, H.L.; Buonassisi, T.; Bristowe, P.D.; Cheetham, A.K. Enhanced visible light absorption for lead-free double perovskite Cs2AgSbBr6. *Chem. Commun.* **2019**, *55*, 3721–3724. [CrossRef]

47. Zhang, Z.; Liang, Y.; Huang, H.; Liu, X.; Li, Q.; Chen, L.; Xu, D. Stable and Highly Efficient Photocatalysis with Lead-Free Double-Perovskite of Cs2AgBiBr6. *Angew. Chem. Int. Ed.* **2019**, *58*, 7263–7267. [CrossRef]

48. Weng, Z.; Qin, J.; Umar, A.A.; Wang, J.; Zhang, X.; Wang, H.; Cui, X.; Li, X.; Zheng, L.; Zhan, Y. Lead-Free Cs2BiAgBr6 Double Perovskite-Based Humidity Sensor with Superfast Recovery Time. *Adv. Funct. Mater.* **2019**, *29*, 1902234. [CrossRef]

49. Yang, J.; Bao, C.; Ning, W.; Wu, B.; Ji, F.; Yan, Z.; Tao, Y.; Liu, J.-M.; Sum, T.C.; Bai, S.; et al. Stable, High-Sensitivity and Fast-Response Photodetectors Based on Lead-Free Cs2AgBiBr6 Double Perovskite Films. *Adv. Opt. Mater.* **2019**, *7*, 1801732. [CrossRef]

50. Worley, C.; Yangui, A.; Roccanova, R.; Du, M.-H.; Saparov, B. (CH3NH3)AuX4·H2O (X = Cl, Br) and (CH3NH3)AuCl4: Low-Band Gap Lead-Free Layered Gold Halide Perovskite Materials. *Chem.–A Eur. J.* **2019**, *25*, 9875–9884. [CrossRef]

51. Pious, J.K.; Katre, A.; Muthu, C.; Chakraborty, S.; Krishna, S.; Nair, V.C. Zero-Dimensional Lead-Free Hybrid Perovskite-like Material with a Quantum-Well Structure. *Chem. Mater.* **2019**, *31*, 1941–1945. [CrossRef]

52. Zhang, R.; Mao, X.; Yang, Y.; Yang, S.; Zhao, W.; Wumaier, T.; Wei, D.; Deng, W.; Han, K. Air-Stable, Lead-Free Zero-Dimensional Mixed Bismuth-Antimony Perovskite Single Crystals with Ultra-broadband Emission. *Angew. Chem.* **2019**, *131*, 2751–2755. [CrossRef]

53. Ding, N.; Zhou, D.; Pan, G.; Xu, W.; Chen, X.; Li, D.; Zhang, X.; Zhu, J.; Ji, Y.; Song, H. Europium-Doped Lead-Free Cs3Bi2Br9 Perovskite Quantum Dots and Ultrasensitive Cu2+ Detection. *ACS Sustain. Chem. Eng.* **2019**, *7*, 8397–8404. [CrossRef]

54. Zhang, Z.-X.; Li, C.; Lu, Y.; Tong, X.-W.; Liang, F.-X.; Zhao, X.-Y.; Wu, D.; Xie, C.; Luo, L.-B. Sensitive Deep Ultraviolet Photodetector and Image Sensor Composed of Inorganic Lead-Free Cs3Cu2I5 Perovskite with Wide Bandgap. *J. Phys. Chem. Lett.* **2019**, *10*, 5343–5350. [CrossRef]

55. Moon, B.J.; Kim, S.J.; Lee, S.; Lee, A.; Lee, H.; Lee, D.S.; Kim, T.-W.; Lee, S.-K.; Bae, S.; Lee, S.H. Rare-Earth-Element-Ytterbium-Substituted Lead-Free Inorganic Perovskite Nanocrystals for Optoelectronic Applications. *Adv. Mater.* **2019**, *31*, 1901716. [CrossRef]

56. Chen, M.; Ju, M.G.; Garces, H.F.; Carl, A.D.; Ono, L.K.; Hawash, Z.; Zhang, Y.; Shen, T.; Qi, Y.; Grimm, R.L.; et al. Highly stable and efficient all-inorganic lead-free perovskite solar cells with native-oxide passivation. *Nat. Commun.* **2019**, *10*. [CrossRef]

57. Li, B.; Zhou, T.; Fang, X.; Zhang, W.; Li, X.; Guan, Z.; Li, J.; Wang, L.; Hark, S.; Zhang, Z. Temperature dependent geometry in perovskite microcrystals for whispering gallery and Fabry-Pérot mode lasing. *J. Mater. Chem. C* **2019**, *7*, 4102–4108. [CrossRef]

58. Geng, C.; Xu, S.; Zhong, H.; Rogach, A.L.; Bi, W. Aqueous synthesis of methylammonium lead halide perovskite nanocrystals. *Angew. Chem. Int. Ed.* **2018**, *57*, 9650–9654. [CrossRef]

59. Liang, P.; Zhang, P.; Pan, A.; Yan, K.; Zhu, Y.; Yang, M.; He, L. Unusual Stability and Temperature-Dependent Properties of Highly Emissive CsPbBr3 Perovskite Nanocrystals Obtained from in Situ Crystallization in Poly(vinylidene difluoride). *ACS Appl. Mater. Interfaces* **2019**, *11*, 22786–22793. [CrossRef]

60. Malgras, V.; Tominaka, S.; Ryan, J.W.; Henzie, J.; Takei, T.; Ohara, K.; Yamauchi, Y. Observation of Quantum Confinement in Monodisperse Methylammonium Lead Halide Perovskite Nanocrystals Embedded in Mesoporous Silica. *J. Am. Chem. Soc.* **2016**, *138*, 13874–13881. [CrossRef]

61. Tan, Y.; Zou, Y.; Wu, L.; Huang, Q.; Yang, D.; Chen, M.; Ban, M.; Wu, C.; Wu, T.; Bai, S.; et al. Highly Luminescent and Stable Perovskite Nanocrystals with Octylphosphonic Acid as a Ligand for Efficient Light-Emitting Diodes. *ACS Appl. Mater. Interfaces* **2018**, *10*, 3784–3792. [CrossRef]

62. Krieg, F.; Ochsenbein, S.T.; Yakunin, S.; Ten Brinck, S.; Aellen, P.; Süess, A.; Clerc, B.; Guggisberg, D.; Nazarenko, O.; Shynkarenko, Y.; et al. Colloidal CsPbX3 (X = Cl, Br, I) Nanocrystals 2.0: Zwitterionic Capping Ligands for Improved Durability and Stability. *ACS Energy Lett.* **2018**, *3*, 641–646. [CrossRef]

63. Ushakova, E.V.; Matuhina, A.I.; Sokolova, A.V.; Cherevkov, S.A.; Dubavik, A.; Medvedev, O.S.; Litvin, A.P.; Kurdyukov, D.A.; Golubev, V.G.; Baranov, A.V. Enhanced stability of the optical responses from all-inorganic perovskite nanocrystals embedded in a synthetic opal matrix. *Nanotechnology* **2019**, *30*, 405206. [CrossRef]

64. Tong, X.W.; Kong, W.Y.; Wang, Y.Y.; Zhu, J.M.; Luo, L.B.; Wang, Z.H. High-Performance Red-Light Photodetector Based on Lead-Free Bismuth Halide Perovskite Film. *ACS Appl. Mater. Interfaces* **2017**, *9*, 18977–18985. [CrossRef]

65. Roknuzzaman, M.; Ostrikov, K.K.; Wang, H.; Du, A.; Tesfamichael, T. Towards lead-free perovskite photovoltaics and optoelectronics by ab-initio simulations. *Sci. Rep.* **2017**, *7*, 1–8. [CrossRef]

66. Khanna, V.K. *Fundamentals of Solid-State Lighting: LEDs, OLEDs, and Their Applications in Illumination and Displays*; CRC Press Taylor & Francis Group: Boca Raton, FL, USA, 2014.

67. Song, J.; Fang, T.; Li, J.; Xu, L.; Zhang, F.; Han, B.; Shan, Q.; Zeng, H. Organic–Inorganic Hybrid Passivation Enables Perovskite QLEDs with an EQE of 16.48%. *Adv. Mater.* **2018**, *30*, 1805409. [CrossRef]

68. Van Le, Q.; Jang, H.W.; Kim, S.Y. Recent Advances toward High-Efficiency Halide Perovskite Light-Emitting Diodes: Review and Perspective. *Small Methods* **2018**, *2*, 1700419. [CrossRef]

69. Veldhuis, S.A.; Boix, P.P.; Yantara, N.; Li, M.; Sum, T.C.; Mathews, N.; Mhaisalkar, S.G. Perovskite Materials for Light-Emitting Diodes and Lasers. *Adv. Mater.* **2016**, *28*, 6804–6834. [CrossRef]

70. Wei, Y.; Cheng, Z.; Lin, J. Correction: An overview on enhancing the stability of lead halide perovskite quantum dots and their applications in phosphor-converted LEDs. *Chem. Soc. Rev.* **2019**, *48*, 405. [CrossRef]

71. Quan, L.N.; Rand, B.P.; Friend, R.H.; Mhaisalkar, S.G.; Lee, T.-W.; Sargent, E.H. Perovskites for Next-Generation Optical Sources. *Chem. Rev.* **2019**, *119*, 7444–7477. [CrossRef]

72. Zhang, X.; Cao, W.; Wang, W.; Xu, B.; Liu, S.; Dai, H.; Chen, S.; Wang, K.; Sun, X.W. Efficient light-emitting diodes based on green perovskite nanocrystals with mixed-metal cations. *Nano Energy* **2016**, *30*, 511–516. [CrossRef]

73. Singh, A.; Chiu, N.-C.; Boopathi, K.M.; Lu, Y.-J.; Mohapatra, A.; Li, G.; Chen, Y.-F.; Guo, T.-F.; Chu, C.-W. Lead-Free Antimony-Based Light-Emitting Diodes through the Vapor–Anion-Exchange Method. *ACS Appl. Mater. Interfaces* **2019**, *11*, 35088–35094. [CrossRef]

74. Luo, J.; Wang, X.; Li, S.; Liu, J.; Guo, Y.; Niu, G.; Yao, L.; Fu, Y.; Gao, L.; Dong, Q.; et al. Efficient and stable emission of warm-white light from lead-free halide double perovskites. *Nature* **2018**, *563*, 541–545. [CrossRef]

75. Zhang, X.; Wang, C.; Zhang, Y.; Zhang, X.; Wang, S.; Lu, M.; Cui, H.; Kershaw, S.V.; Yu, W.W.; Rogach, A.L. Bright Orange Electroluminescence from Lead-Free Two-Dimensional Perovskites. *ACS Energy Lett.* **2019**, *4*, 242–248. [CrossRef]

76. Wang, A.; Guo, Y.; Zhou, Z.; Niu, X.; Wang, Y.; Muhammad, F.; Li, H.; Zhang, T.; Wang, J.; Nie, S.; et al. Aqueous acid-based synthesis of lead-free tin halide perovskites with near-unity photoluminescence quantum efficiency. *Chem. Sci.* **2019**, *10*, 4573–4579. [CrossRef]

77. Yang, Z.; Jiang, Z.; Liu, X.; Zhou, X.; Zhang, J.; Li, W. Bright Blue Light-Emitting Doped Cesium Bromide Nanocrystals: Alternatives of Lead-Free Perovskite Nanocrystals for White LEDs. *Adv. Opt. Mater.* **2019**, *7*, 1–8. [CrossRef]

78. Schawlow, A.L.; Townes, C.H. Infrared and optical masers. *Phys. Rev.* **1958**, *112*, 1940–1949. [CrossRef]

79. Maiman, T.H.; Hoskins, R.H.; D'Haenens, I.J.; Asawa, C.K.; Evtuhov, V. Stimulated optical emission in fluorescent solids. II. Spectroscopy and stimulated emission in ruby. *Phys. Rev.* **1961**, *123*, 1151–1157. [CrossRef]

80. Maiman, T.H. Stimulated optical radiation in Ruby. *Nature* **1960**, *187*, 493–494. [CrossRef]

81. Wang, K.; Wang, S.; Xiao, S.; Zhang, N.; Wang, Y.; Yang, W.; Wang, Y.; Zhang, C.; Sun, W.; Song, Q. Single-Crystalline Perovskite Microlasers for High-Contrast and Sub-Diffraction Imaging. *Adv. Funct. Mater.* **2019**, *29*, 1904868. [CrossRef]

82. Wang, J.; Da, P.; Zhang, Z.; Luo, S.; Liao, L.; Sun, Z.; Shen, X.; Wu, S.; Zheng, G.; Chen, Z. Lasing from lead halide perovskite semiconductor microcavity system. *Nanoscale* **2018**, *10*, 10371–10376. [CrossRef]

83. Liu, Z.; Yang, J.; Du, J.; Hu, Z.; Shi, T.; Zhang, Z.; Liu, Y.; Tang, X.; Leng, Y.; Li, R. Robust Subwavelength Single-Mode Perovskite Nanocuboid Laser. *ACS Nano* **2018**, *12*, 5923–5931. [CrossRef] [PubMed]

84. Weng, G.; Xue, J.; Tian, J.; Hu, X.; Bao, X.; Lin, H.; Chen, S.; Zhu, Z.; Chu, J. Picosecond Random Lasing Based on Three-Photon Absorption in Organometallic Halide CH3NH3PbBr3 Perovskite Thin Films. *ACS Photonics* **2018**, *5*, 2951–2959. [CrossRef]

85. Du, W.; Zhang, S.; Wu, Z.; Shang, Q.; Mi, Y.; Chen, J.; Qin, C.; Qiu, X.; Zhang, Q.; Liu, X. Unveiling lasing mechanism in CsPbBr3 microsphere cavities. *Nanoscale* **2019**, *11*, 3138–3144. [CrossRef] [PubMed]

86. Kondo, T.; Azuma, T.; Yuasa, T.; Ito, R. Biexciton lasing in the layered perovskite-type material (C6H13NH3)2PbI4. *Solid State Commun.* **1998**, *105*, 253–255. [CrossRef]

87. Liu, F.; Zhang, Y.; Ding, C.; Kobayashi, S.; Izuishi, T.; Nakazawa, N.; Toyoda, T.; Ohta, T.; Hayase, S.; Minemoto, T.; et al. Highly Luminescent Phase-Stable CsPbI 3 Perovskite Quantum Dots Achieving Near 100% Absolute Photoluminescence Quantum Yield. *ACS Nano* **2017**, *11*, 10373–10383. [CrossRef]

88. Safdar, A.; Wang, Y.; Krauss, T.F. Random lasing in solution-processed perovskite thin films. *Opt. InfoBase Conf. Pap.* **2017**, *26*, 75–84.

89. Li, Z.; Moon, J.; Gharajeh, A.; Haroldson, R.; Hawkins, R.; Hu, W.; Zakhidov, A.; Gu, Q. Room-temperature continuous-wave operation of organometal halide perovskite lasers. *ACS Nano* **2018**, *12*, 10968–10976. [CrossRef]

90. Mathies, F.; Brenner, P.; Hernandez-Sosa, G.; Howard, I.A.; Paetzold, U.W.; Lemmer, U. Inkjet-printed perovskite distributed feedback lasers. *Opt. Express* **2018**, *26*, A144. [CrossRef]

91. Jäckle, M.; Linnenbank, H.; Hentschel, M.; Saliba, M.; Tikhodeev, S.G.; Giessen, H. Tunable green lasing from circular grating distributed feedback based on CH 3 NH 3 PbBr 3 perovskite. *Opt. Mater. Express* **2019**, *9*, 2006–2021. [CrossRef]

92. Weng, G.; Tian, J.; Chen, S.; Xue, J.; Yan, J.; Hu, X.; Chen, S.; Zhu, Z.; Chu, J. Giant reduction of the random lasing threshold in CH3NH3PbBr3 perovskite thin films by using a patterned sapphire substrate. *Nanoscale* **2019**, *11*, 10636–10645. [CrossRef]

93. Guo, P.; Hossain, M.K.; Shen, X.; Sun, H.; Yang, W.; Liu, C.; Ho, C.Y.; Kwok, C.K.; Tsang, S.W.; Luo, Y.; et al. Room-Temperature Red–Green–Blue Whispering-Gallery Mode Lasing and White-Light Emission from Cesium Lead Halide Perovskite (CsPbX 3, X = Cl, Br, I) Microstructures. *Adv. Opt. Mater.* **2018**, *6*, 1700993. [CrossRef]

94. Hu, Z.; Liu, Z.; Bian, Y.; Liu, D.; Tang, X.; Hu, W.; Zang, Z.; Zhou, M.; Sun, L.; Tang, J.; et al. Robust Cesium Lead Halide Perovskite Microcubes for Frequency Upconversion Lasing. *Adv. Opt. Mater.* **2017**, *5*, 1700419. [CrossRef]

95. Zhou, B.; Dong, H.; Jiang, M.; Zheng, W.; Sun, L.; Zhao, B.; Tang, B.; Pan, A.; Zhang, L. Single-mode lasing and 3D confinement from perovskite micro-cubic cavity. *J. Mater. Chem. C* **2018**, *6*, 11740–11748. [CrossRef]

96. Zhou, B.; Jiang, M.; Dong, H.; Zheng, W.; Huang, Y.; Han, J.; Pan, A.; Zhang, L. High-Temperature Upconverted Single-Mode Lasing in 3D Fully Inorganic Perovskite Microcubic Cavity. *ACS Photonics* **2019**, *6*, 793–801. [CrossRef]

97. Mi, Y.; Liu, Z.; Shang, Q.; Niu, X.; Shi, J.; Zhang, S.; Chen, J.; Du, W.; Wu, Z.; Wang, R.; et al. Fabry–Pérot Oscillation and Room Temperature Lasing in Perovskite Cube-Corner Pyramid Cavities. *Small* **2018**, *14*, 1703136. [CrossRef]

98. Zhao, X.; He, D.-W.; Wang, Y.-S.; Hu, Y.; Fu, C.; Li, X. Label-free tungsten disulfide quantum dots as a fluorescent sensing platform for highly efficient detection of copper (II) ions. *Chin. Phys. B* **2017**, *26*, 066102. [CrossRef]

99. Zhang, N.; Fan, Y.; Wang, K.; Gu, Z.; Wang, Y.; Ge, L.; Xiao, S.; Song, Q. All-optical control of lead halide perovskite microlasers. *Nat. Commun.* **2019**, *10*, 1770. [CrossRef]

100. Liu, X.; Niu, L.; Wu, C.; Cong, C.; Wang, H.; Zeng, Q.; He, H.; Fu, Q.; Fu, W.; Yu, T.; et al. Periodic Organic–Inorganic Halide Perovskite Microplatelet Arrays on Silicon Substrates for Room-Temperature Lasing. *Adv. Sci.* **2016**, *3*, 1600137. [CrossRef]

101. Fu, Y.; Zhu, H.; Stoumpos, C.C.; Ding, Q.; Wang, J.; Kanatzidis, M.G.; Zhu, X.; Jin, S. Broad Wavelength Tunable Robust Lasing from Single-Crystal Nanowires of Cesium Lead Halide Perovskites (CsPbX3, X = Cl, Br, I). *ACS Nano* **2016**, *10*, 7963–7972. [CrossRef]

102. Evans, T.J.S.; Schlaus, A.; Fu, Y.; Zhong, X.; Atallah, T.L.; Spencer, M.S.; Brus, L.E.; Jin, S.; Zhu, X.Y. Continuous-Wave Lasing in Cesium Lead Bromide Perovskite Nanowires. *Adv. Opt. Mater.* **2018**, *6*, 1700982. [CrossRef]

103. Zhao, J.; Yan, Y.; Wei, C.; Zhang, W.; Gao, Z.; Zhao, Y.S. Switchable Single-Mode Perovskite Microlasers Modulated by Responsive Organic Microdisks. *Nano Lett.* **2018**, *18*, 1241–1245. [CrossRef] [PubMed]

104. Schlaus, A.P.; Spencer, M.S.; Miyata, K.; Liu, F.; Wang, X.; Datta, I.; Lipson, M.; Pan, A.; Zhu, X.Y. How lasing happens in CsPbBr 3 perovskite nanowires. *Nat. Commun.* **2019**, *10*, 265. [CrossRef] [PubMed]

105. Tang, B.; Dong, H.; Sun, L.; Zheng, W.; Wang, Q.; Sun, F.; Jiang, X.; Pan, A.; Zhang, L. Single-Mode Lasers Based on Cesium Lead Halide Perovskite Submicron Spheres. *ACS Nano* **2017**, *11*, 10681–10688. [CrossRef] [PubMed]

106. Zheng, Z.; Wang, X.; Shen, Y.; Luo, Z.; Li, L.; Gan, L.; Ma, Y.; Li, H.; Pan, A.; Zhai, T. Space-Confined Synthesis of 2D All-Inorganic CsPbI 3 Perovskite Nanosheets for Multiphoton-Pumped Lasing. *Adv. Opt. Mater.* **2018**, *6*, 1800879. [CrossRef]

107. Huang, C.; Sun, W.; Liu, S.; Li, S.; Wang, S.; Wang, Y.; Zhang, N.; Fu, H.; Xiao, S.; Song, Q. Highly Controllable Lasing Actions in Lead Halide Perovskite–Si 3 N 4 Hybrid Micro-Resonators. *Laser Photonics Rev.* **2019**, *13*, 1800189. [CrossRef]

108. Zhizhchenko, A.; Syubaev, S.; Berestennikov, A.; Yulin, A.V.; Porfirev, A.; Pushkarev, A.; Shishkin, I.; Golokhvast, K.; Bogdanov, A.A.; Zakhidov, A.A.; et al. Single-Mode Lasing from Imprinted Halide-Perovskite Microdisks. *ACS Nano* **2019**, *13*, 4140–4147. [CrossRef]

109. Wang, Y.; Gu, Z.; Ren, Y.; Wang, Z.; Yao, B.; Dong, Z.; Adamo, G.; Zeng, H.; Sun, H. Perovskite-Ion Beam Interactions: Toward Controllable Light Emission and Lasing. *ACS Appl. Mater. Interfaces* **2019**, *11*, 15756–15763. [CrossRef]

110. Booker, E.P.; Price, M.B.; Budden, P.J.; Abolins, H.; del Valle-Inclan Redondo, Y.; Eyre, L.; Nasrallah, I.; Phillips, R.T.; Friend, R.H.; Deschler, F.; et al. Vertical Cavity Biexciton Lasing in 2D Dodecylammonium Lead Iodide Perovskites. *Adv. Opt. Mater.* **2018**, *6*, 1–5. [CrossRef]

111. Raghavan, C.M.; Chen, T.P.; Li, S.S.; Chen, W.L.; Lo, C.Y.; Liao, Y.M.; Haider, G.; Lin, C.C.; Chen, C.C.; Sankar, R.; et al. Low-Threshold Lasing from 2D Homologous Organic-Inorganic Hybrid Ruddlesden-Popper Perovskite Single Crystals. *Nano Lett.* **2018**, *18*, 3221–3228. [CrossRef]

112. Liang, Y.; Shang, Q.; Wei, Q.; Zhao, L.; Liu, Z.; Shi, J.; Zhong, Y.; Chen, J.; Gao, Y.; Li, M.; et al. Lasing from Mechanically Exfoliated 2D Homologous Ruddlesden–Popper Perovskite Engineered by Inorganic Layer Thickness. *Adv. Mater.* **2019**, *31*, 1903030. [CrossRef]

113. Zhai, W.; Tian, C.; Yuan, K.; Ge, C.; Zhao, S.; Yu, H.; Li, Y.; Chen, W.; Ran, G. Optically pumped lasing of segregated quasi-2D perovskite microcrystals in vertical microcavity at room temperature. *Appl. Phys. Lett.* **2019**, *114*, 131107. [CrossRef]

114. Wang, Y.; Li, X.; Nalla, V.; Zeng, H.; Sun, H. Solution-Processed Low Threshold Vertical Cavity Surface Emitting Lasers from All-Inorganic Perovskite Nanocrystals. *Adv. Funct. Mater.* **2017**, *27*, 1605088. [CrossRef]

115. Lin, C.H.; Zeng, Q.; Lafalce, E.; Yu, S.; Smith, M.J.; Yoon, Y.J.; Chang, Y.; Jiang, Y.; Lin, Z.; Vardeny, Z.V.; et al. Large-Area Lasing and Multicolor Perovskite Quantum Dot Patterns. *Adv. Opt. Mater.* **2018**, *6*, 1800474. [CrossRef]

116. Fan, T.; Lü, J.; Chen, Y.; Yuan, W.; Huang, Y. Random lasing in cesium lead bromine perovskite quantum dots film. *J. Mater. Sci. Mater. Electron.* **2019**, *30*, 1084–1088. [CrossRef]

117. Tang, X.; Hu, Z.; Chen, W.; Xing, X.; Zang, Z.; Hu, W.; Qiu, J.; Du, J.; Leng, Y.; Jiang, X.; et al. Room temperature single-photon emission and lasing for all-inorganic colloidal perovskite quantum dots. *Nano Energy* **2016**, *28*, 462–468. [CrossRef]

118. Yuan, S.; Chen, D.; Li, X.; Zhong, J.; Xu, X. In Situ Crystallization Synthesis of CsPbBr3 Perovskite Quantum Dot-Embedded Glasses with Improved Stability for Solid-State Lighting and Random Upconverted Lasing. *ACS Appl. Mater. Interfaces* **2018**, *10*, 18918–18926. [CrossRef] [PubMed]

119. Wang, L.; Meng, L.; Chen, L.; Huang, S.; Wu, X.; Dai, G.; Deng, L.; Han, J.; Zou, B.; Zhang, C.; et al. Ultralow-Threshold and Color-Tunable Continuous-Wave Lasing at Room-Temperature from in Situ Fabricated Perovskite Quantum Dots. *J. Phys. Chem. Lett.* **2019**, *10*, 3248–3253. [CrossRef]

120. Pourdavoud, N.; Haeger, T.; Mayer, A.; Cegielski, P.J.; Giesecke, A.L.; Heiderhoff, R.; Olthof, S.; Zaefferer, S.; Shutsko, I.; Henkel, A.; et al. Room-Temperature Stimulated Emission and Lasing in Recrystallized Cesium Lead Bromide Perovskite Thin Films. *Adv. Mater.* **2019**, *31*, 1903717. [CrossRef]

121. Brenner, P.; Bar-On, O.; Jakoby, M.; Allegro, I.; Richards, B.S.; Paetzold, U.W.; Howard, I.A.; Scheuer, J.; Lemmer, U. Continuous wave amplified spontaneous emission in phase-stable lead halide perovskites. *Nat. Commun.* **2019**, *10*, 988. [CrossRef]

122. Li, G.; Price, M.; Deschler, F. Research Update: Challenges for high-efficiency hybrid lead-halide perovskite LEDs and the path towards electrically pumped lasing. *APL Mater.* **2016**, *4*, 091507. [CrossRef]

123. Li, M.; Wei, Q.; Muduli, S.K.; Yantara, N.; Xu, Q.; Mathews, N.; Mhaisalkar, S.G.; Xing, G.; Sum, T.C. Enhanced Exciton and Photon Confinement in Ruddlesden–Popper Perovskite Microplatelets for Highly Stable Low-Threshold Polarized Lasing. *Adv. Mater.* **2018**, *30*, 1707235. [CrossRef] [PubMed]

124. Yu, H.; Cheng, X.; Wang, Y.; Liu, Y.; Rong, K.; Li, Z.; Wan, Y.; Gong, W.; Watanabe, K.; Taniguchi, T.; et al. Waterproof Perovskite-Hexagonal Boron Nitride Hybrid Nanolasers with Low Lasing Thresholds and High Operating Temperature. *ACS Photonics* **2018**, *5*, 4520–4528. [CrossRef]

125. Huang, L.; Gao, Q.; Sun, L.D.; Dong, H.; Shi, S.; Cai, T.; Liao, Q.; Yan, C.H. Composition-Graded Cesium Lead Halide Perovskite Nanowires with Tunable Dual-Color Lasing Performance. *Adv. Mater.* **2018**, *30*, 1800596. [CrossRef] [PubMed]

126. Xing, G.; Kumar, M.H.; Chong, W.K.; Liu, X.; Cai, Y.; Ding, H.; Asta, M.; Grätzel, M.; Mhaisalkar, S.; Mathews, N.; et al. Solution-Processed Tin-Based Perovskite for Near-Infrared Lasing. *Adv. Mater.* **2016**, *28*, 8191–8196. [CrossRef]

127. Chen, L.J.; Dai, J.H.; Lin, J.D.; Mo, T.S.; Lin, H.P.; Yeh, H.C.; Chuang, Y.C.; Jiang, S.A.; Lee, C.R. Wavelength-Tunable and Highly Stable Perovskite-Quantum-Dot-Doped Lasers with Liquid Crystal Lasing Cavities. *ACS Appl. Mater. Interfaces* **2018**, *10*, 33307–33315. [CrossRef]